

10295

NACA TN 3957

0067006



TECH LIBRARY KAFB, NM

# NATIONAL ADVISORY COMMITTEE FOR AERONAUTICS

TECHNICAL NOTE 3957

SOME EFFECTS OF TAIL HEIGHT AND WING PLAN FORM ON THE  
STATIC LONGITUDINAL STABILITY CHARACTERISTICS OF  
A SMALL-SCALE MODEL AT HIGH SUBSONIC SPEEDS

By Albert G. Few, Jr., and Thomas J. King, Jr.

Langley Aeronautical Laboratory  
Langley Field, Va.



Washington

May 1957

AFMDC  
TECHNICAL LIBRARY  
AFL 2811



0067006

## TECHNICAL NOTE 3957

SOME EFFECTS OF TAIL HEIGHT AND WING PLAN FORM ON THE  
STATIC LONGITUDINAL STABILITY CHARACTERISTICS OF  
A SMALL-SCALE MODEL AT HIGH SUBSONIC SPEEDS<sup>1</sup>

By Albert G. Few, Jr., and Thomas J. King, Jr.

## SUMMARY

An investigation has been made in the Langley high-speed 7- by 10-foot tunnel to determine some effects of tail height and wing plan form on the static longitudinal stability characteristics of a complete, small-scale model at high subsonic speeds. The model had both a low-tail position (wing chord plane extended) and a high-tail position (65 percent semispan above the wing chord plane extended). The wings were 4 percent thick, had an aspect ratio of 3, and had various taper ratios and angles of sweep. Three wings had a taper ratio of 0.50 and quarter-chord sweep angles of 25°, 30°, and 35°; whereas the fourth wing had 30° of sweep and a taper ratio of 0.20. The Mach number range extended from about 0.80 to 0.94 with corresponding Reynolds numbers ranging from about  $1.17 \times 10^6$  to  $1.29 \times 10^6$  for average test conditions.

The drag due to lift increases with increasing sweep through the Mach number range. Some increase in drag due to lift is evident with decrease in taper ratio for wings having 30° of sweep through most of the speed range.

In relation to the pitch-up problem in the speed range investigated herein, no very definite advantage of any of the wing plan forms was realized for the tail-off configurations. At low Mach numbers ( $M = 0.80$ ), the high-tail configuration provides, in general, the most nearly linear pitching-moment curves at angles of attack below approximately 16° for all wing plan forms. Unstable breaks occurred above this angle of attack for all wing plan forms at the lower Mach numbers, but not at the highest test Mach number. The low-tail arrangement provides, in general, stable breaks and fairly linear pitching-moment curves above an angle of attack of approximately 4° for all wing plan forms at the low Mach numbers but not at the highest test Mach number.

<sup>1</sup>Supersedes recently declassified NACA Research Memorandum L54G12 by Albert G. Few, Jr., and Thomas J. King, Jr., 1954.

## INTRODUCTION

Some present-day aircraft, both research and production types, having highly sweptback wings, exhibit undesirable pitch-up tendencies at low and moderate lift coefficients through both the subsonic and transonic speed ranges. These characteristics can make it difficult to employ the aircraft as a satisfactory gun platform under certain conditions. In addition, the design load factor can be exceeded as a result of the pitch-up caused by nonlinearities in the pitching-moment curve. In general, satisfactory pitching-moment characteristics are obtained only by giving due consideration to many factors - such as, aspect ratio (ref. 1), thickness ratio, sweep angle, tail location, and the wing leading-edge configuration.

The purpose of this investigation was to determine the effects of variation in wing sweep angle between  $25^\circ$  and  $35^\circ$  on the longitudinal stability characteristics of a model at high subsonic speeds and also to determine the extent to which these characteristics may be altered by various tail locations.

Four wings having an aspect ratio of 3, NACA 65A004 airfoil sections parallel to the free stream, various angles of sweep with respect to the quarter-chord line, and various taper ratios were used in the investigation. Three of these wings had a taper ratio of 0.50 and quarter-chord sweep angles of  $25^\circ$ ,  $30^\circ$ , and  $35^\circ$ ; whereas the fourth wing had  $30^\circ$  of sweep and a taper ratio of 0.20. The test Mach number ranged from about 0.80 to 0.94 with corresponding Reynolds numbers ranging from about  $1.17 \times 10^6$  to  $1.29 \times 10^6$ .

## SYMBOLS

The system of stability axes employed, together with an indication of the positive direction of forces, moments, and angles, is shown in figure 1. The center of moments is located at the 25-percent mean aerodynamic chord of the wing. The symbols are defined as follows:

$C_L$	lift coefficient, $Lift/qS$
$C_m$	pitching-moment coefficient, $Pitching\ moment/qS\bar{c}$
$\Delta C_D$	total drag coefficient minus drag coefficient at zero lift
$q$	dynamic pressure, $\rho V^2/2$ , lb/sq ft
$C_{L_\alpha}$	lift-curve slope
$\beta$	angle of sideslip, deg

y	distance from plane of symmetry
D	diameter
$\rho$	mass density of air, slugs/cu ft
V	free-stream velocity, fps
S	wing area, sq ft
A	aspect ratio, $b^2/S$
b	wing span, ft
$\bar{c}$	wing mean aerodynamic chord, $\frac{2}{S} \int_0^{b/2} c^2 dy$ , ft
c	wing chord at any spanwise station, ft
$c_r$	wing-root chord, ft
$c_t$	wing-tip chord, ft
$\lambda$	taper ratio
$i_t$	angle of stabilizer incidence, trailing edge down for positive deflection, deg
$\alpha$	angle of attack, deg
$\Lambda_c/4$	wing sweep angle about quarter-chord line, deg
M	Mach number of free stream
R	radius

## MODEL DESIGNATIONS

W	wing
F	fuselage
V	vertical tail
$H_H$	high-horizontal-tail configuration ( $0.65b/2$ above chord plane)
$H_L$	low-horizontal-tail configuration (on chord plane)

## MODEL AND APPARATUS

Details of the complete model as tested are given in figure 2 and a photograph of the model mounted on the sting-type support system is shown as figure 3. With this sting-support system, the model can be remotely operated through an angle-of-attack range from about  $-2^\circ$  to  $24^\circ$ . All wings were constructed of stainless steel, had NACA 65A004 airfoil sections parallel to the free stream, and had an aspect ratio of 3. Three of the wings had a taper ratio of 0.50 and quarter-chord sweep angles of  $25^\circ$ ,  $30^\circ$ , and  $35^\circ$ ; whereas the fourth wing had  $30^\circ$  of sweep and a taper ratio of 0.20. The model could be tested with both a low- and high-horizontal-tail arrangement. The low horizontal tail, with incidence fixed at  $0^\circ$ , was mounted on the center line of the fuselage which was in the plane of the wing chord; whereas, the high horizontal tail (with possible  $0^\circ$  and  $-6^\circ$  incidence settings) was mounted on the vertical tail as a T-tail configuration. The high tail was 3.39 inches above the wing chord plane, which corresponds to about 65 percent of the wing semispan. The fuselage had a fineness ratio of 10.94 and was constructed of stainless steel. Its geometric characteristics, including afterbody ordinates, are given in figure 4. A six-component electrical strain-gage balance was mounted internally in the fuselage to measure the forces and moments presented herein.

## TESTS AND CORRECTIONS

Tests were made in the Langley high-speed 7- by 10-foot tunnel through a Mach number range from about 0.80 to 0.94, which corresponds to a Reynolds number range from about  $1.17 \times 10^6$  to  $1.29 \times 10^6$  based on a wing mean aerodynamic chord of 0.299 foot. Angles of attack from  $-2^\circ$  to  $24^\circ$  were obtained at the lower Mach numbers. The angle-of-attack range at  $M = 0.94$  was limited, in general, to about  $15^\circ$  so as not to exceed the maximum design load of the balance. No evidence of tunnel choking occurred at the highest Mach number and angle of attack. Jet-boundary corrections determined by the method of reference 2 and blocking corrections by the method of reference 3 were negligible and, therefore, were not applied to the data. The angle of attack, however, has been corrected for deflection of the sting-support system and balance under load.

## RESULTS AND DISCUSSION

### Presentation of Results

Aerodynamic characteristics of the various model configurations are presented as follows:

## Figures

## Basic data:

$\Lambda_c/4 = 25^\circ$ , $\lambda = 0.50$ . . . . .	5 to 7
$\Lambda_c/4 = 30^\circ$ , $\lambda = 0.50$ and $0.20$ . . . . .	8 to 10
$\Lambda_c/4 = 35^\circ$ , $\lambda = 0.50$ . . . . .	11 to 13
Fuselage alone . . . . .	14

## Summary of aerodynamic characteristics:

Effect of wing plan form on $C_{L\alpha}$ , tail off . . . . .	15
Effect of wing plan form on drag due to lift, tail off . . . . .	16
Effect of tail height on pitching-moment characteristics . . . . .	17
Effect of tail height and wing plan form on the shape of pitching-moment curves . . . . .	18
Effect of tail height on aerodynamic center . . . . .	19

The basic drag polars have not been presented inasmuch as the balance drag gages were not sufficiently sensitive to measure accurately the small forces encountered at zero lift. This deficiency, however, is not believed to affect the validity of comparisons of the drag due to lift for the various wing plan forms.

## Lift and Drag Characteristics

Lift-curve slopes averaged over a lift-coefficient range of  $\pm 0.10$  are presented in figure 15 for the range of wing-plan-form variables investigated. Throughout the Mach number range, no particularly significant changes in  $\partial C_L / \partial \alpha$  are evident. However, the  $30^\circ$  swept wing having a taper ratio of 0.20 provides some increase in lift-curve slope (as would be expected from ref. 4) over that obtained with the other plan forms throughout most of the Mach number range.

The drag due to lift through the Mach number range and for the range of plan-form variables investigated is presented for the tail-off configurations in figure 16. Also shown in figure 16 ( $M = 0.80$ ) is the theoretical induced drag  $C_L^2 / \pi A$ . It will be noted that the drag is considerably higher than theory for all the plan forms tested, probably because of the leading-edge separation associated with the sharp leading edges of these thin wings. The effect of sweep on the drag due to lift is as would be expected - that is, an increase with an increase in wing sweep throughout the Mach number range - since it is the component of the flow normal to the wing that determines to a large extent the chordwise pressure distributions (ref. 5) and thereby the separation effects. The  $30^\circ$  swept wing with a taper ratio of 0.20 indicated considerable increases in drag due to lift over that which was realized with wings having a taper ratio of 0.50 below a Mach number of 0.94. This is probably due, in part at

least, to the fact that the leading-edge sweep is greatest for this wing and, therefore, has a greater effect on the leading-edge separation.

### Longitudinal Stability Characteristics

The data presented in figures 5 to 13 show, in general, that, for the range of wing plan forms and horizontal-tail heights investigated, nonlinearities in the pitching-moment curves of the familiar pitch-up type existed throughout the Mach number range. In order to provide a more direct comparison of the effects of tail height on these nonlinearities in the pitching-moment curves for the various wing plan forms, comparisons of the data are presented in figure 17 for Mach numbers of 0.80 and 0.94. The results indicate considerably less stability contributed by the low tail than by the high tail at low angles of attack, probably because of the fact that the low tail is in a stronger downwash field than the high tail. At moderate angles of attack, the stability contributed by both the high and low horizontal tails is somewhat comparable. At angles of attack above approximately  $16^\circ$ , however, the pitching moment contributed by the high tail decreases rapidly, and results in a pitch-up for the complete configuration; whereas the low-tail configuration retains its stability up to the highest angle of attack tested. This is due to the fact that the high tail has moved down into the wing wake where the downwash and loss of dynamic pressure reduce the tail effectiveness, whereas the low tail is moving away from the wing wake. Inasmuch as the tail is carrying considerable load at angles of attack corresponding to the pitch-up and, therefore, is susceptible to the effects of any losses in dynamic pressure, and inasmuch as the configurations were considerably out of trim at these angles of attack, some additional tests were made with the stabilizer set at  $-6^\circ$  incidence which trims the configuration in the region of the pitch-up. The results are presented in figures 7(d), 10(d), and 13(d). These results indicate that the pitch-up is less severe when the tail loads are reduced and that the pitch-up for  $i_t = 0^\circ$  is, therefore, caused in part by a loss in dynamic pressure with increasing angle of attack. The high-tail configurations resulted in pitching-moment curves which are considerably more linear than those of the tail-off configurations (fig. 17 or basic data) which have rather abrupt changes in stability at moderate angles of attack. This fact indicates that a rather abrupt increase in downwash occurs in this angle-of-attack range as the high tail moves into the wing wake. This type of downwash variation is illustrated in figure 12 of reference 6. It should be pointed out, however, that the high tail has a rather large static margin (see fig. 17) and if the tail size had been reduced to provide a more conventional static margin, the stability curve probably would not have been so nearly linear.

It will be noted that there was a rather large out-of-trim (nose up) pitching moment for the high-tail configuration at zero lift, which

corresponds to about  $1.5^\circ$  of flow angularity. This apparently is due to the flow field around the rear end of the fuselage, inasmuch as unpublished wing-off tests of another tail plan form in the same relative position indicate approximately the same angle. The low tail which was mounted in a symmetrical position with respect to the fuselage provided almost no pitching moment at zero angle of attack.

In order to illustrate further the effects of tail height and wing plan form on the pitching-moment behavior, data are presented in figure 18 for all configurations of tail height and wing plan form at Mach numbers of 0.80 and 0.94 with the initial pitching-moment-curve slope adjusted to the constant value of  $-0.05$ . In relation to the pitch-up problem in the speed range investigated, no very definite improvement with variations in sweep or taper ratio is realized from the tail-off moment curves presented in figure 18(a). It can be seen that slight destabilizing tendencies occurred in a fairly low-lift-coefficient range at a Mach number of 0.80 for all the plan forms investigated except for the wing with  $35^\circ$  of sweep which provided about the most linear pitching-moment curve at a Mach number of 0.80. As the Mach number increased, however,  $35^\circ$  of sweep produced an undesirable jog in the moment curve, which is just about coincident with the break in the lift curve (fig. 11(a)). Slight destabilizing tendencies at a Mach number of 0.94 also occurred in the moment curves for the  $30^\circ$  sweptback wings having taper ratios of 0.20 and 0.50; however, these destabilizing trends are present well above the lift break and may be in the region of strong buffet.

The addition of a low horizontal tail, which was located in the plane of the wing chord, did not alter appreciably the destabilizing tendencies noted in the tail-off curves. (Compare fig. 18(a) with fig. 18(b).) At a Mach number of 0.80,  $35^\circ$  of sweep provides about the most nearly linear pitching-moment curves; however, at a Mach number of 0.94, a sudden unstable break occurred but at a slightly higher lift coefficient than for the tail-off case. Destablizing characteristics were noted also at  $M = 0.94$  for the wings with  $30^\circ$  of sweep having taper ratios of 0.20 and 0.50. The  $25^\circ$  swept wing at a Mach number of 0.80 has an unstable tendency well below the lift break, followed by a pronounced increase in stability. At a Mach number of 0.94, however, no unstable tendencies are noted, although the pronounced stable break which occurred at a fairly low lift coefficient is very evident. The characteristics noted for the  $25^\circ$  swept wing with the low-tail configuration were, in general, similar to those of the tail-off condition.

With the horizontal tail located as a T-tail configuration or about 65 percent of the wing semispan above the wing chord plane extended, the pitching-moment curve at a Mach number of 0.80 indicates abrupt instability as the tail enters the wing wake at fairly high lift coefficients (fig. 18(c)). This abrupt unstable change in pitching moment encountered for all wings is preceded, however, by a pronounced stable break which is

in turn well above the lift break and into a probable buffet zone. As the Mach number was increased to 0.94, unstable trends again occurred; and for all plan forms, except possibly the 25° swept wing, these trends are present below the lift break.

Basic fuselage-alone data are presented in figure 14. The fuselage becomes more unstable with increasing lift coefficient and appears to have no abrupt breaks through the speed range investigated. It would seem logical to assume, therefore, that the irregularities associated with the basic wing-fuselage pitching-moment curves (figs. 5 to 13) can be due to wing characteristics.

Longitudinal-stability parameters  $\partial C_m / \partial C_L$  for all configurations of tail heights in conjunction with the various wing plan forms are presented in figure 19. The slopes  $\partial C_m / \partial C_L$  have been averaged over a lift-coefficient range from about  $C_L = 0.10$  to  $C_L = -0.10$ . The low-tail configuration provided little stability in the low Mach number range; and for all wing plan forms tested, except the 30° swept wing having a taper ratio of 0.20, the low tail provided a negative effect at the higher Mach numbers. The low-tail contribution to stability for the 30° swept wing having a taper ratio of 0.20 was small but positive and constant throughout the Mach number range. The tail contribution to stability provided by the high horizontal tail was about constant throughout the Mach number range for the range of variables investigated.

### CONCLUSIONS

The results of an investigation to determine some effects of tail height and wing plan form on the static longitudinal stability characteristics at high subsonic speeds of a small-scale model incorporating 4-percent-thick wings with various taper ratios ( $\lambda = 0.20$  and  $0.50$ ) and quarter-chord sweep angles ( $\Lambda_c/4 = 25^\circ, 30^\circ$ , and  $35^\circ$ ) indicate the following conclusions:

1. The drag due to lift increases with increasing sweep through the Mach number range. Some increases in drag due to lift are indicated with a decrease in taper ratio for wings having 30° of sweep through most of the Mach number range.
2. In relation to the pitch-up problem through the speed range investigated, no very definite advantage of any of the wing plan forms was realized for the tail-off configurations.
3. At low Mach numbers ( $M = 0.80$ ), the high-tail arrangement (65 percent of the semispan above wing chord plane) provides, in general, the most nearly linear pitching-moment curves at angles of attack below approximately  $16^\circ$  for all wing plan forms. Unstable breaks occurred above this

angle of attack for all wing plan forms at the lower Mach numbers, but not at the highest test Mach number. The low-tail arrangement provides, in general, stable breaks and fairly linear pitching-moment curves above an angle of attack of approximately  $4^{\circ}$  for all wing plan forms at the low Mach numbers but not at the highest test Mach number.

Langley Aeronautical Laboratory,  
National Advisory Committee for Aeronautics,  
Langley Field, Va., June 23, 1954.

#### REFERENCES

1. Kuhn, Richard E., and Wiggins, James W.: Wind-Tunnel Investigation of the Aerodynamic Characteristics in Pitch of Wing-Fuselage Combinations at High Subsonic Speeds - Aspect-Ratio Series. NACA RM L52A29, 1952.
2. Gillis, Clarence L., Polhamus, Edward C., and Gray, Joseph L., Jr.: Charts for Determining Jet-Boundary Corrections for Complete Models in 7- By 10-Foot Closed Rectangular Wind Tunnels. NACA WR L-123, 1945. (Formerly NACA ARR L5G31.)
3. Herriot, John G.: Blockage Corrections for Three-Dimensional-Flow Closed-Throat Wind Tunnels, With Consideration of the Effect of Compressibility. NACA Rep. 995, 1950. (Supersedes NACA RM A7B28.)
4. DeYoung, John, and Harper, Charles W.: Theoretical Symmetric Span Loading At Subsonic Speeds for Wings Having Arbitrary Plan Form. NACA Rep. 921, 1948.
5. Jones, Robert T.: Effects of Sweep-Back on Boundary Layer and Separation. NACA Rep. 884, 1947. (Supersedes NACA TN 1402.)
6. Axelson, John A.: Downwash Behind a Triangular Wing of Aspect Ratio 3 - Transonic Bump Method. NACA RM A53I23, 1953.

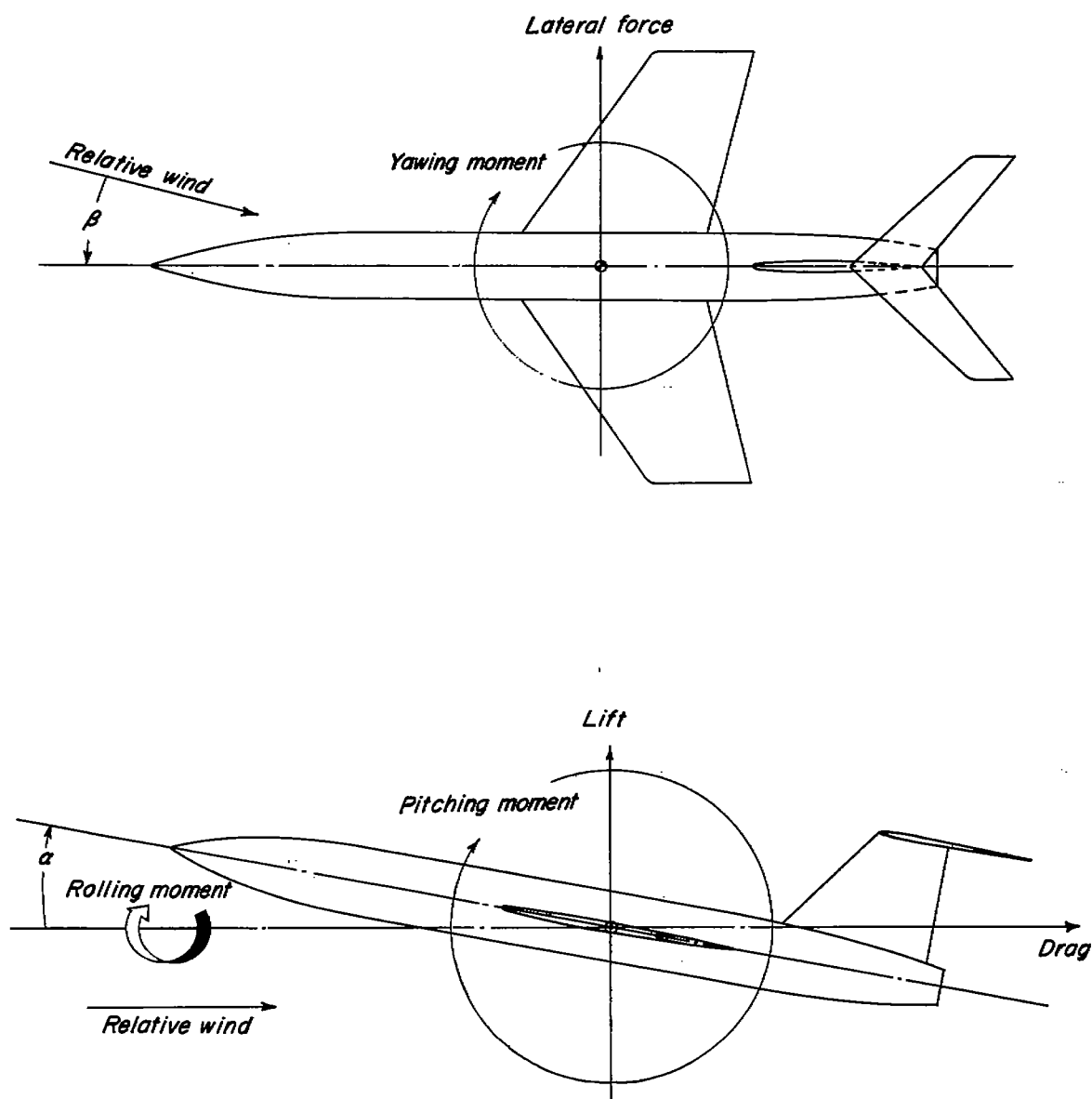
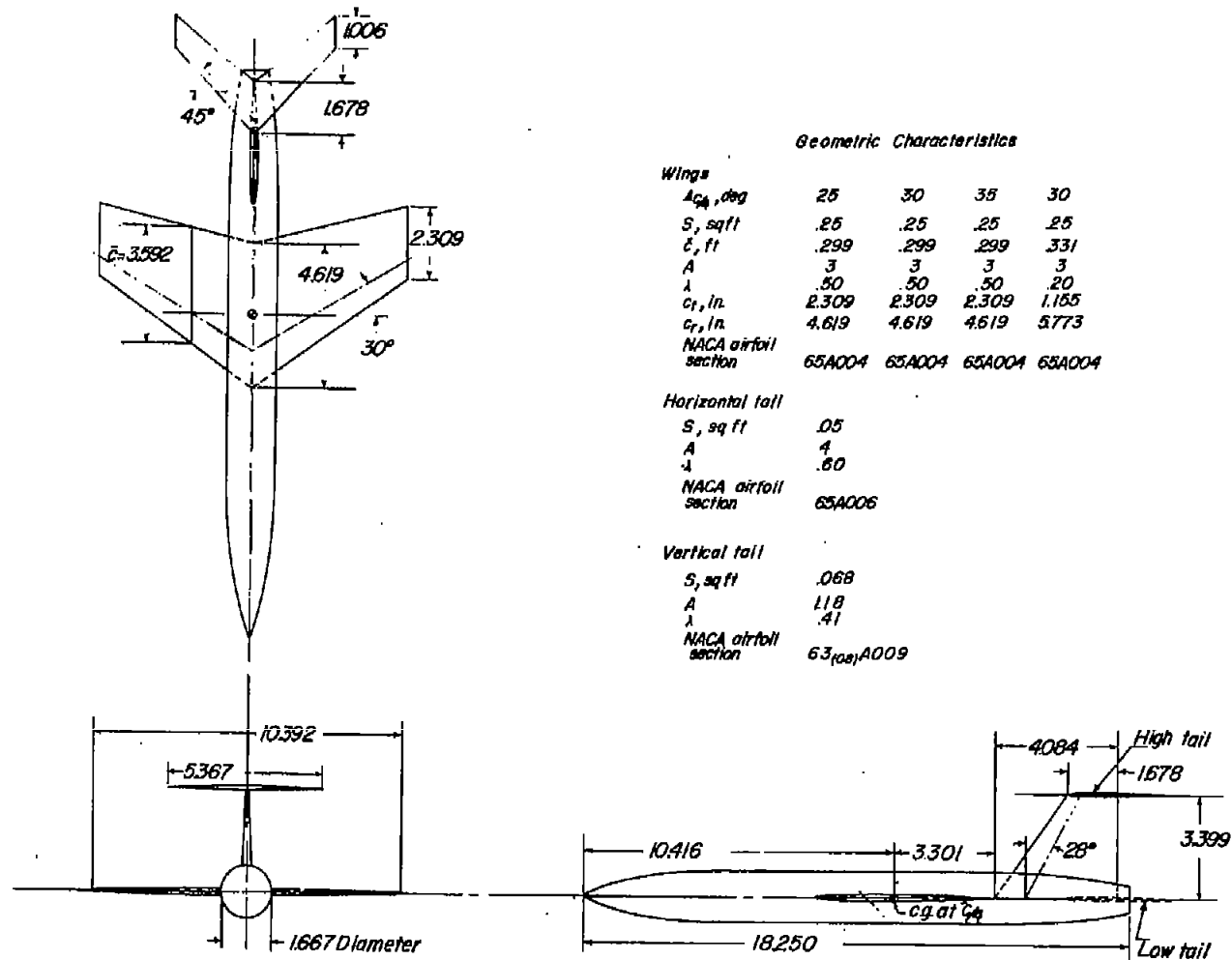
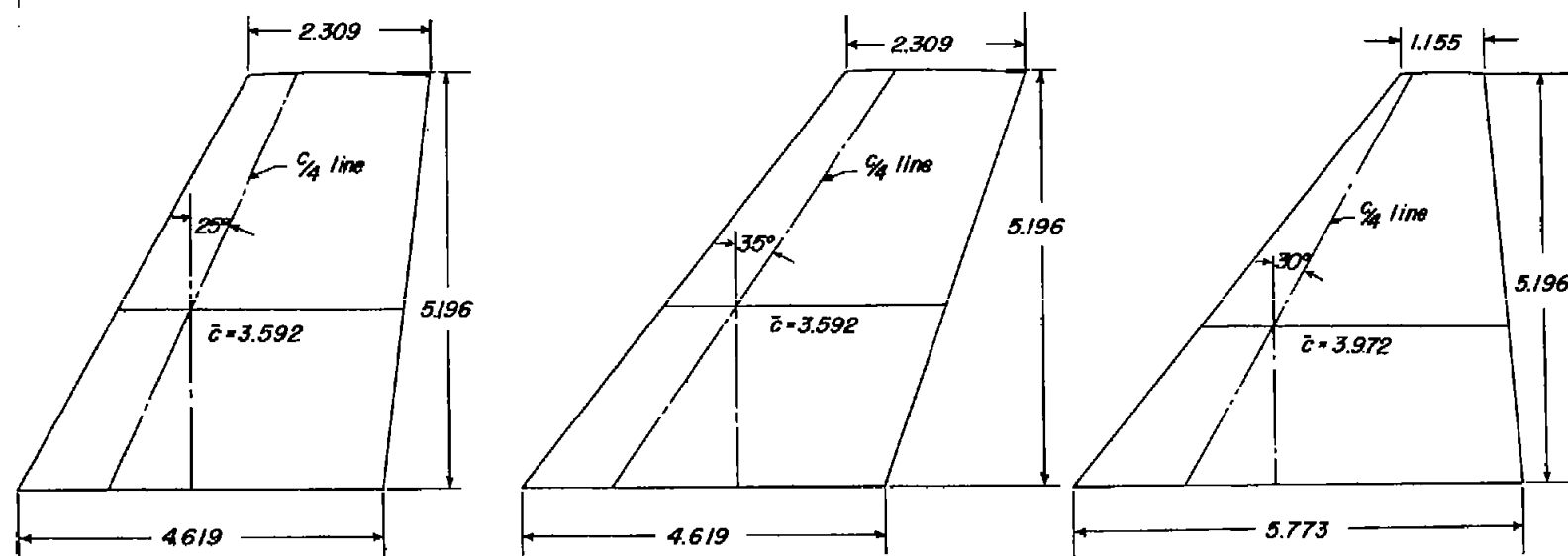


Figure 1.- System of axes. Arrows indicate positive direction of forces, moments, and angles.



(a) Complete model details.

Figure 2.- Details of complete model. All dimensions in inches.



$$\Delta_{C/4} = 25^\circ$$

$$\lambda = 0.50$$

$$\Delta_{C/4} = 35^\circ$$

$$\lambda = 0.50$$

$$\Delta_{C/4} = 30^\circ$$

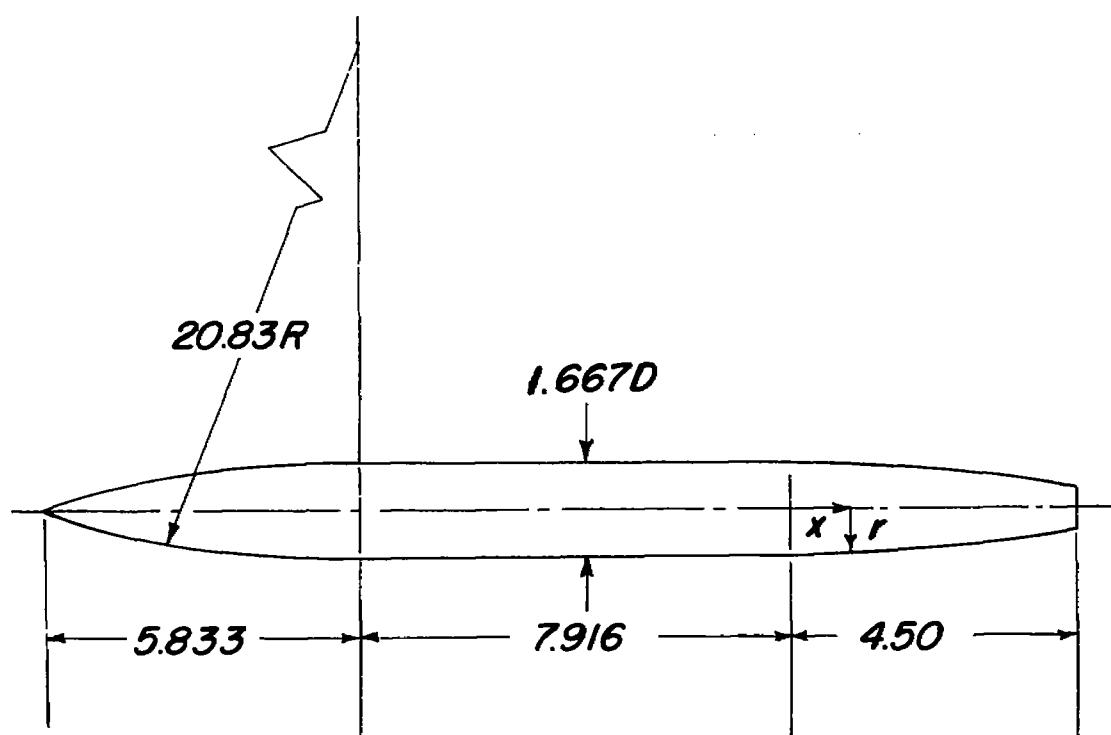
$$\lambda = 0.20$$

(b) Semispan details.

Figure 2.- Concluded.



L-81612  
 Figure 3.- Photograph of model mounted on sting support system in Langley  
 high-speed 7- by 10-foot tunnel.



Afterbody Ordinates, inches	
$x$	$r$
0	.833
.584	.812
1.166	.779
2.166	.712
4.50	.549

Figure 4.- Fuselage ordinates. All dimensions in inches.

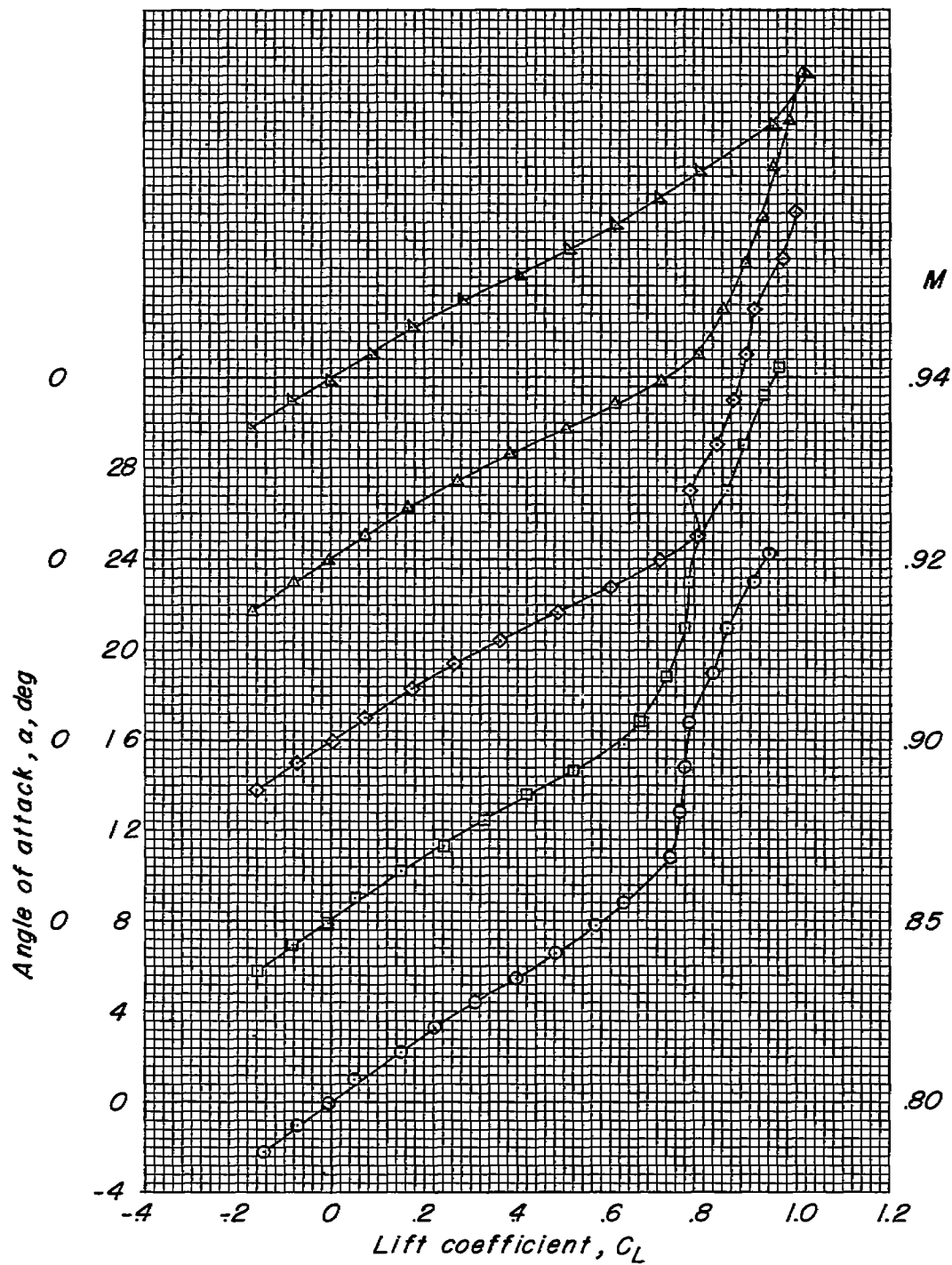
(a) Variation of  $\alpha$  with  $C_L$ .

Figure 5.- Aerodynamic characteristics of wing-fuselage combination.  
 $\Lambda_c/4 = 25^\circ$ ;  $\lambda = 0.50$ .

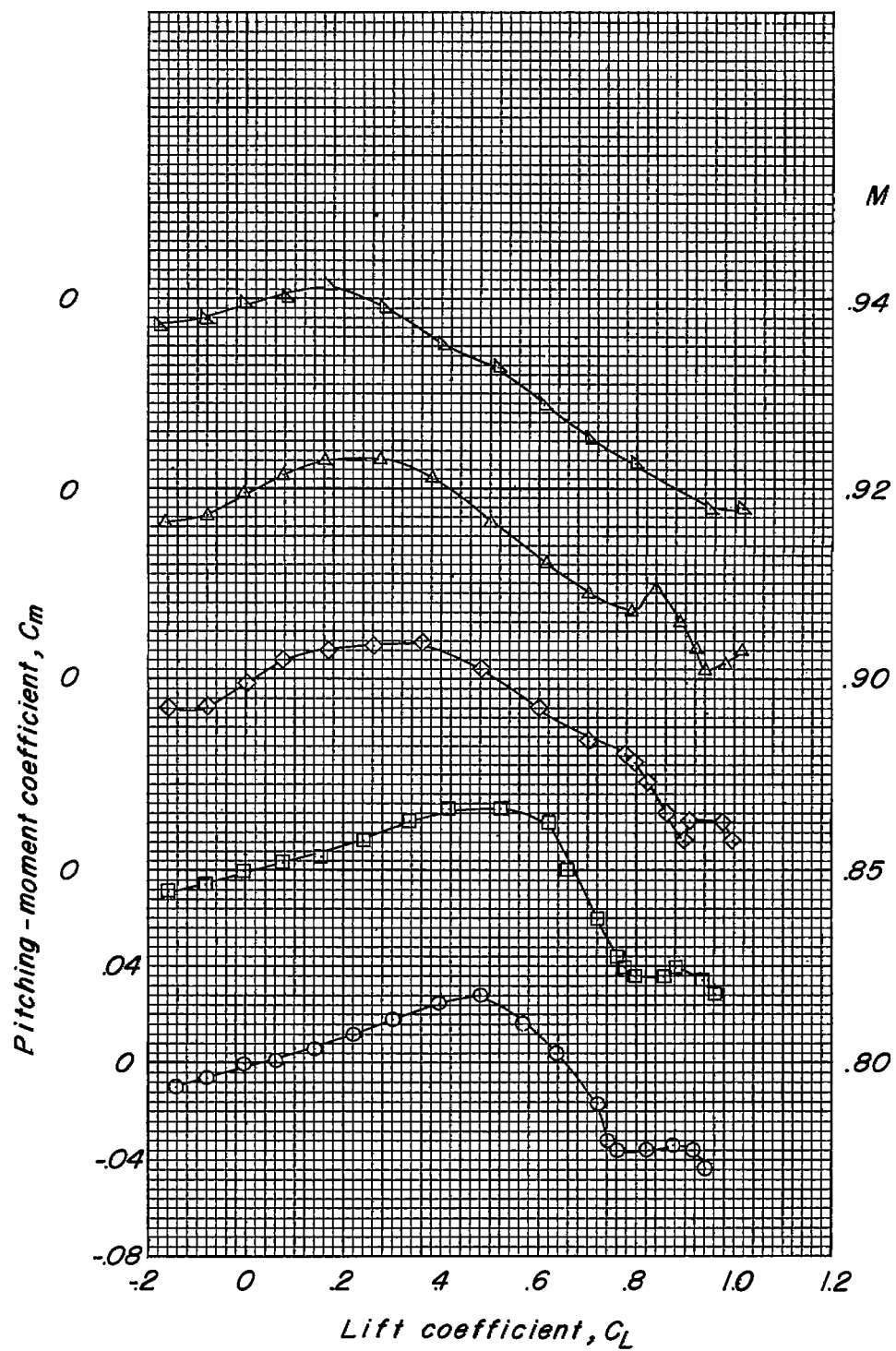
(b) Variation of  $C_m$  with  $C_L$ .

Figure 5.- Continued.

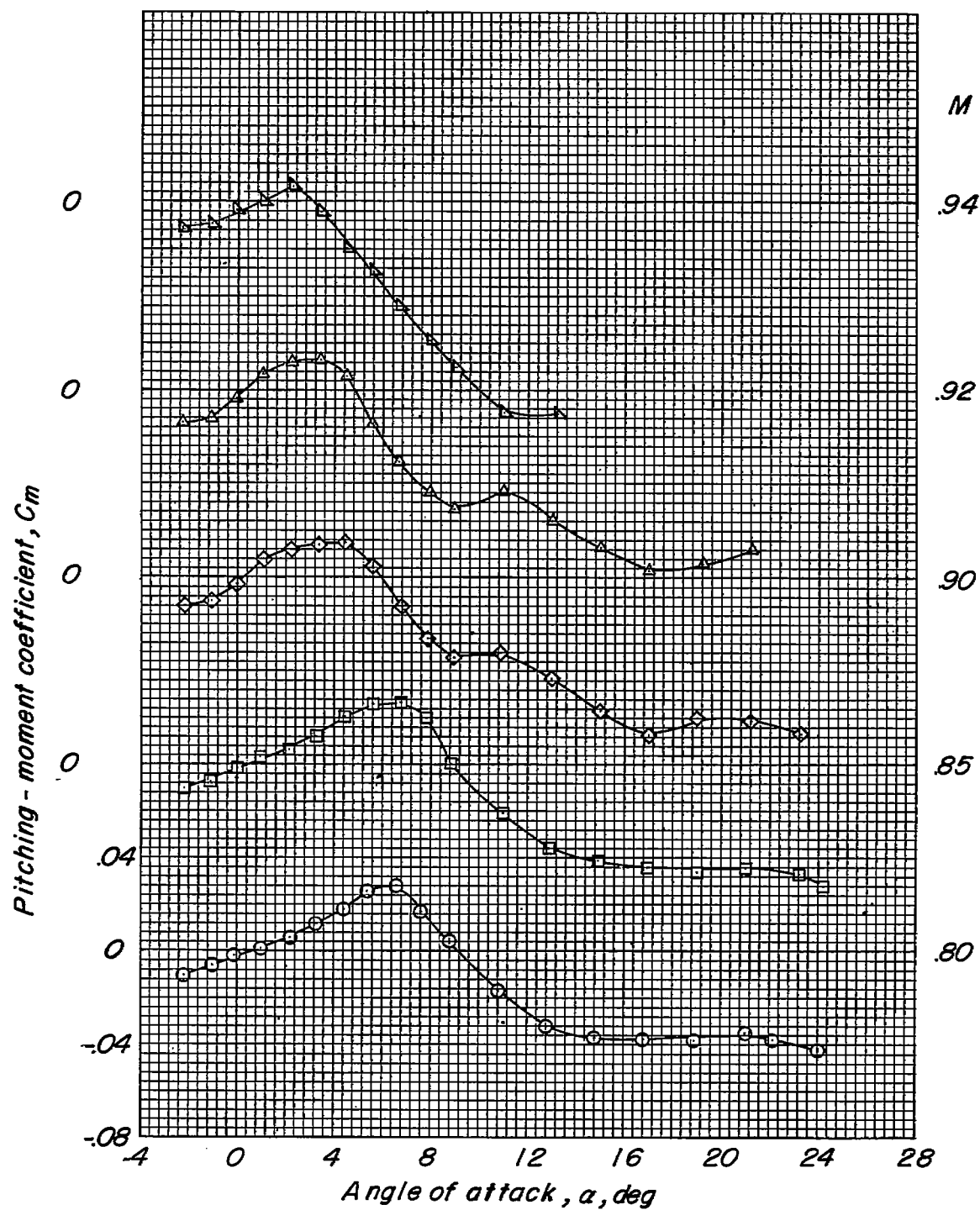
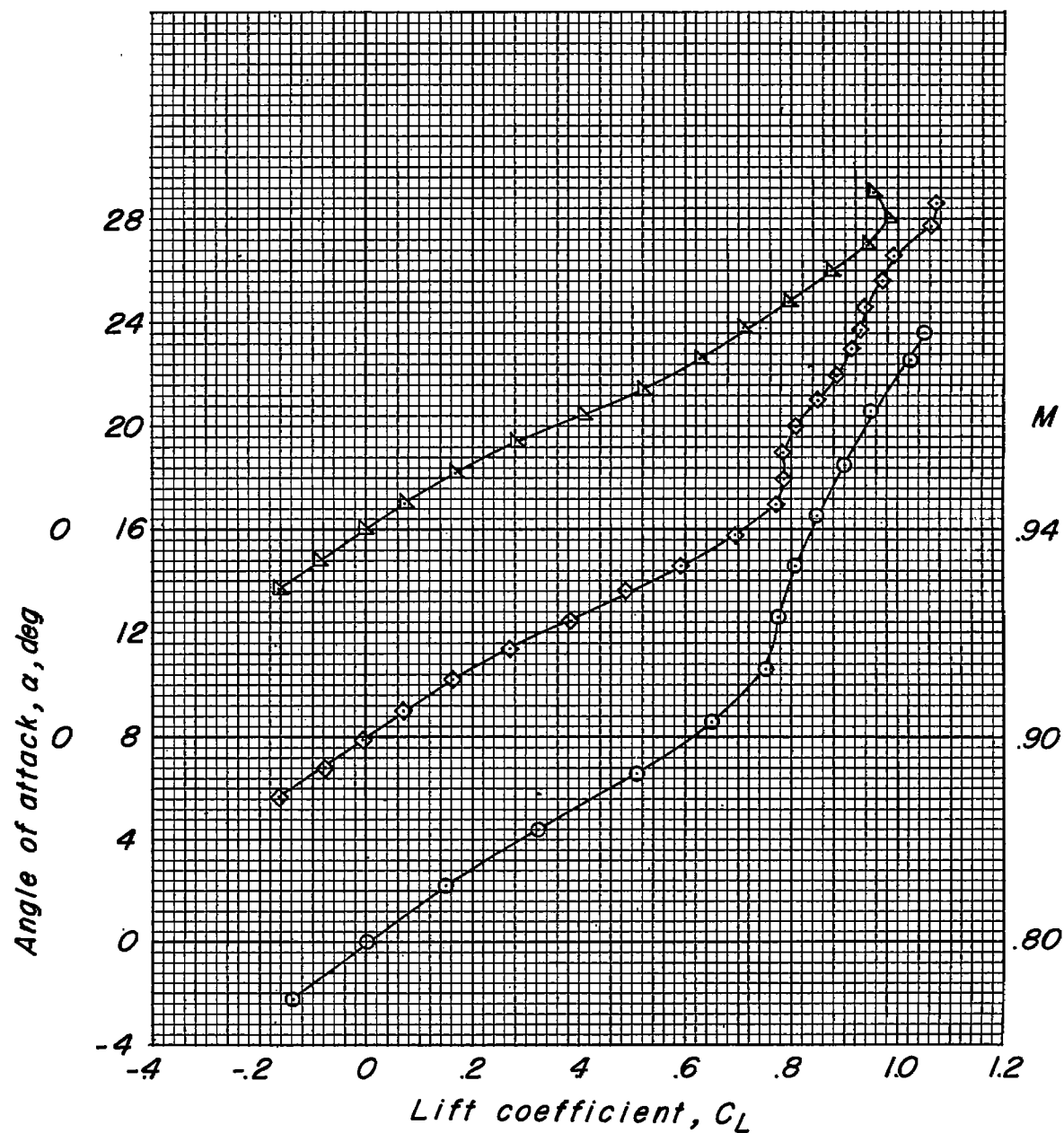
(c) Variation of  $C_m$  with  $\alpha$ .

Figure 5.- Concluded.



(a) Variation of  $\alpha$  with  $C_L$ .

Figure 6.- Aerodynamic characteristics of wing-fuselage-low-tail configuration.  $\Lambda_{c/4} = 25^\circ$ ;  $\lambda = 0.50$ ;  $i_t = 0^\circ$ .

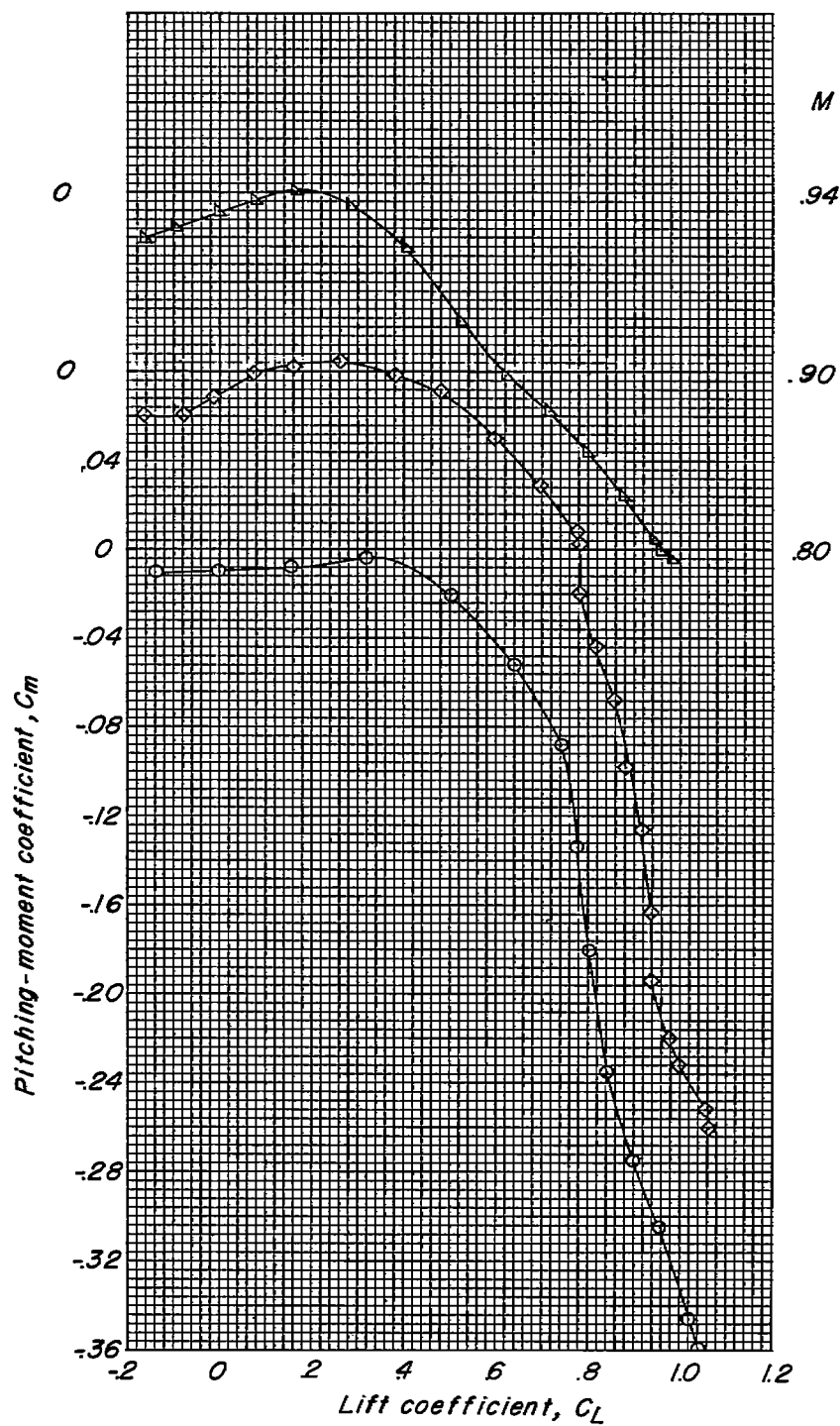
(b) Variation of  $C_m$  with  $C_L$ .

Figure 6.- Continued.

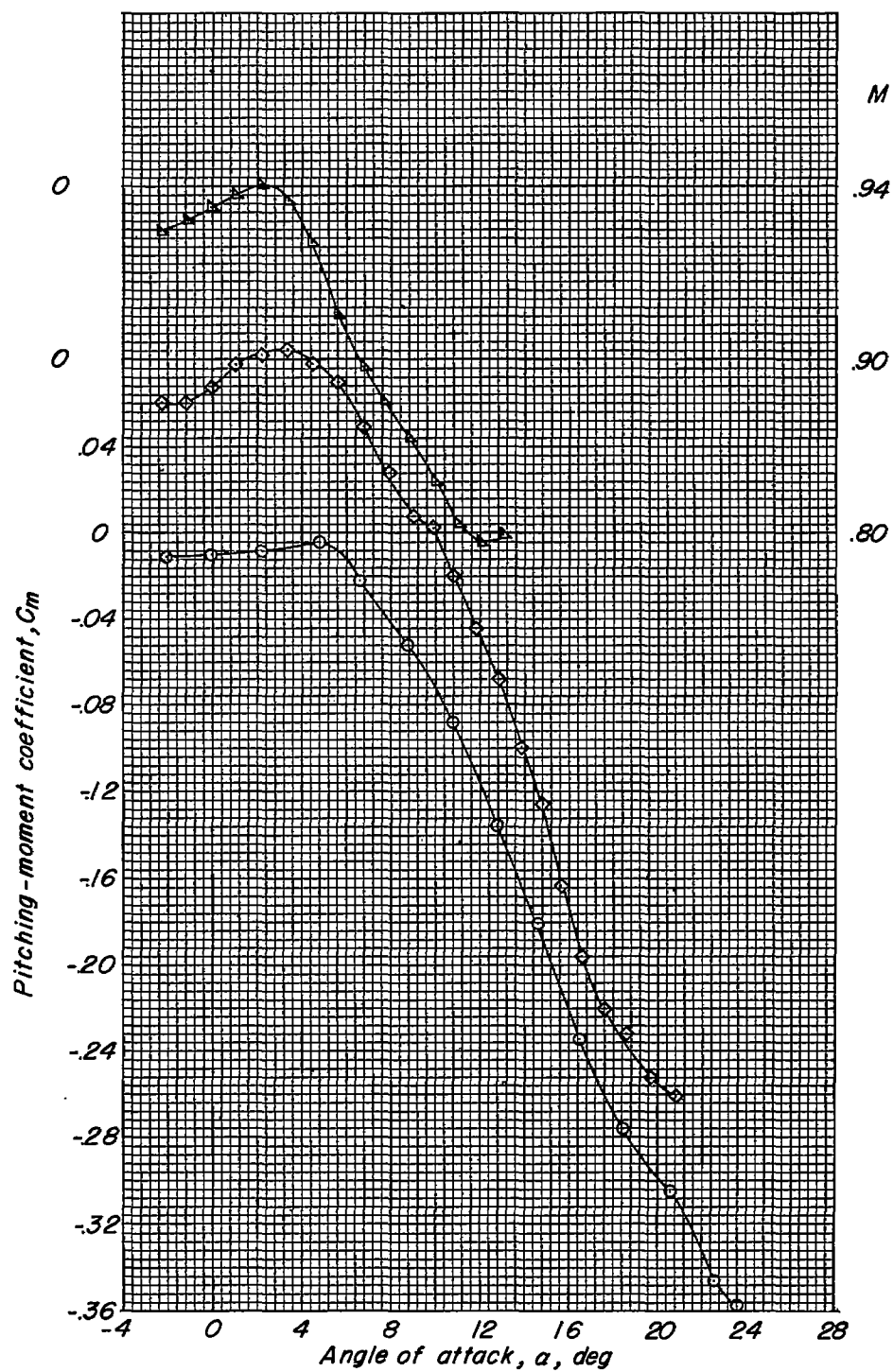
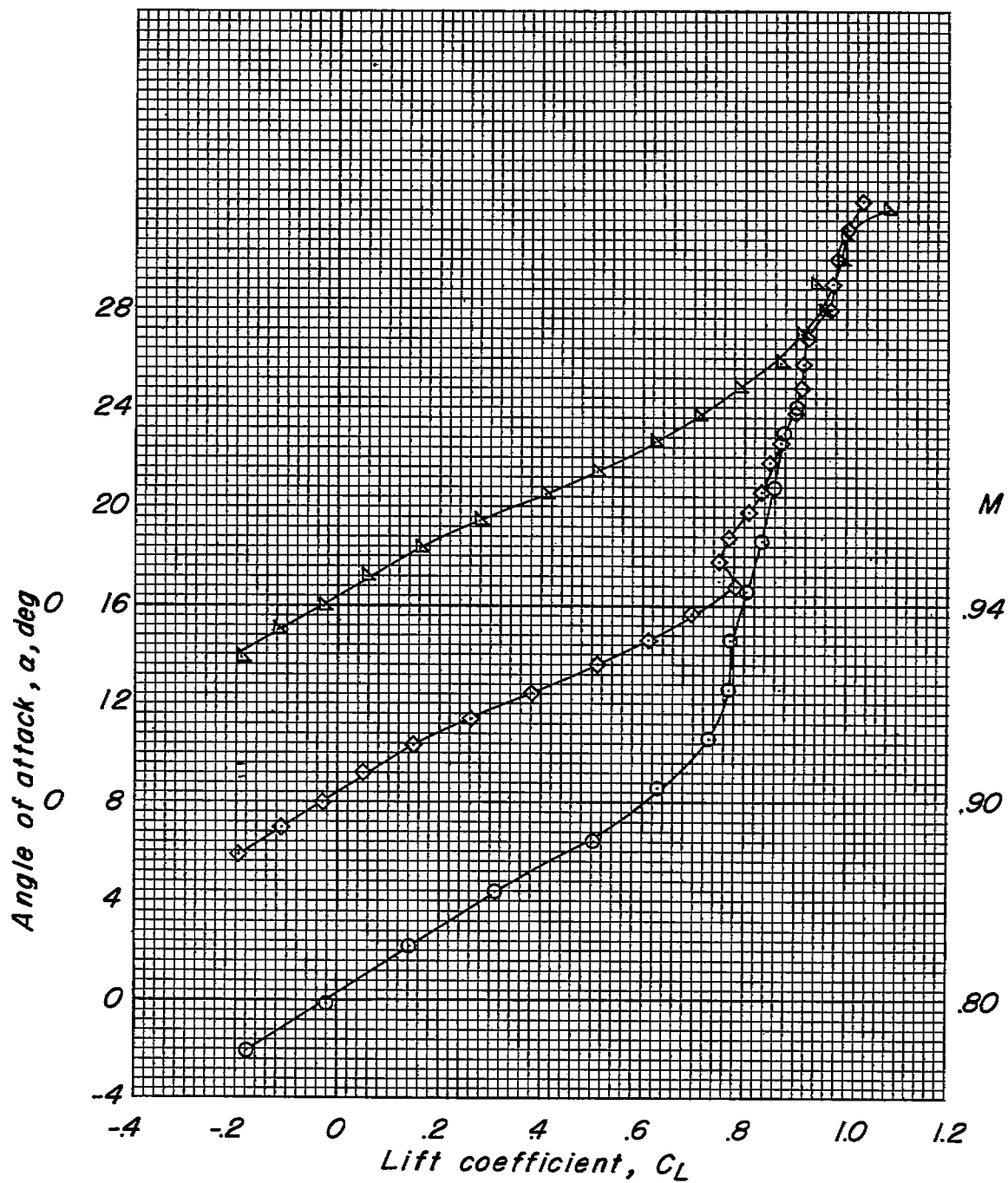
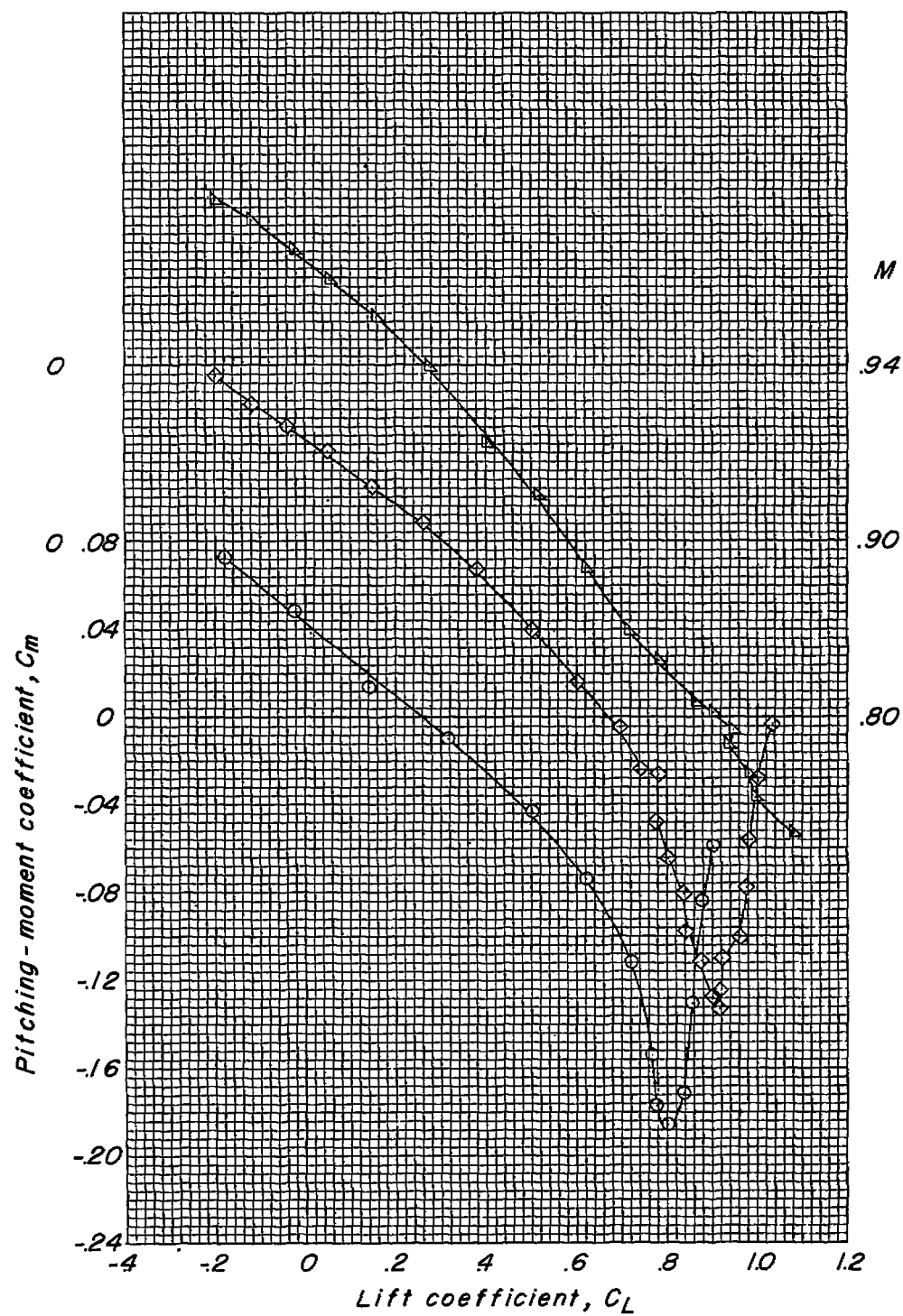
(c) Variation of  $C_m$  with  $\alpha$ .

Figure 6.- Concluded.



(a) Variation of  $\alpha$  with  $C_L$ ;  $i_t = 0^\circ$ .

Figure 7.- Aerodynamic characteristics of wing-fuselage-high-tail configuration.  $\Lambda_c/4 = 25^\circ$ ;  $\lambda = 0.50$ .



(b) Variation of  $C_m$  with  $C_L$ ;  $i_t = 0^\circ$ .

Figure 7.- Continued.

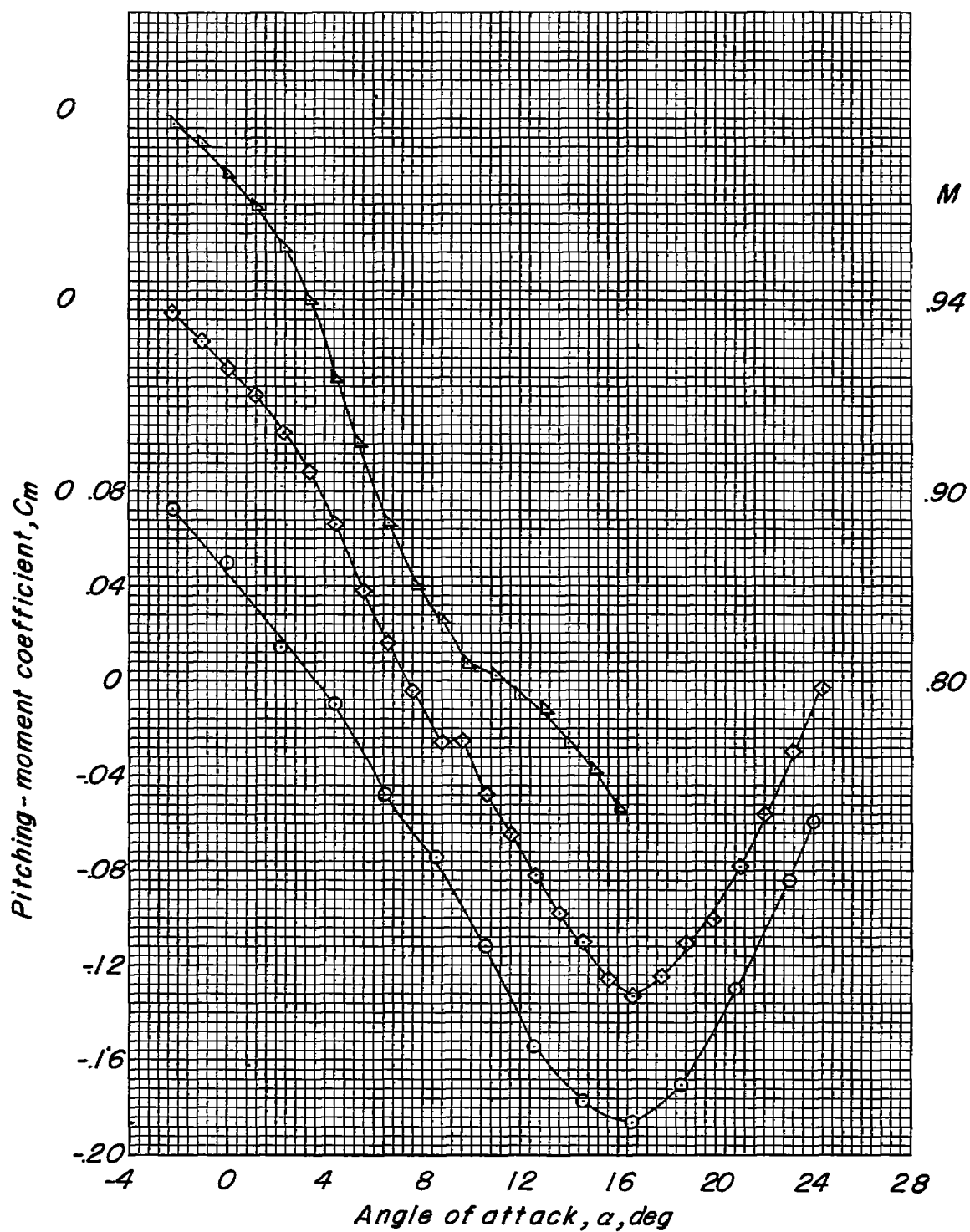
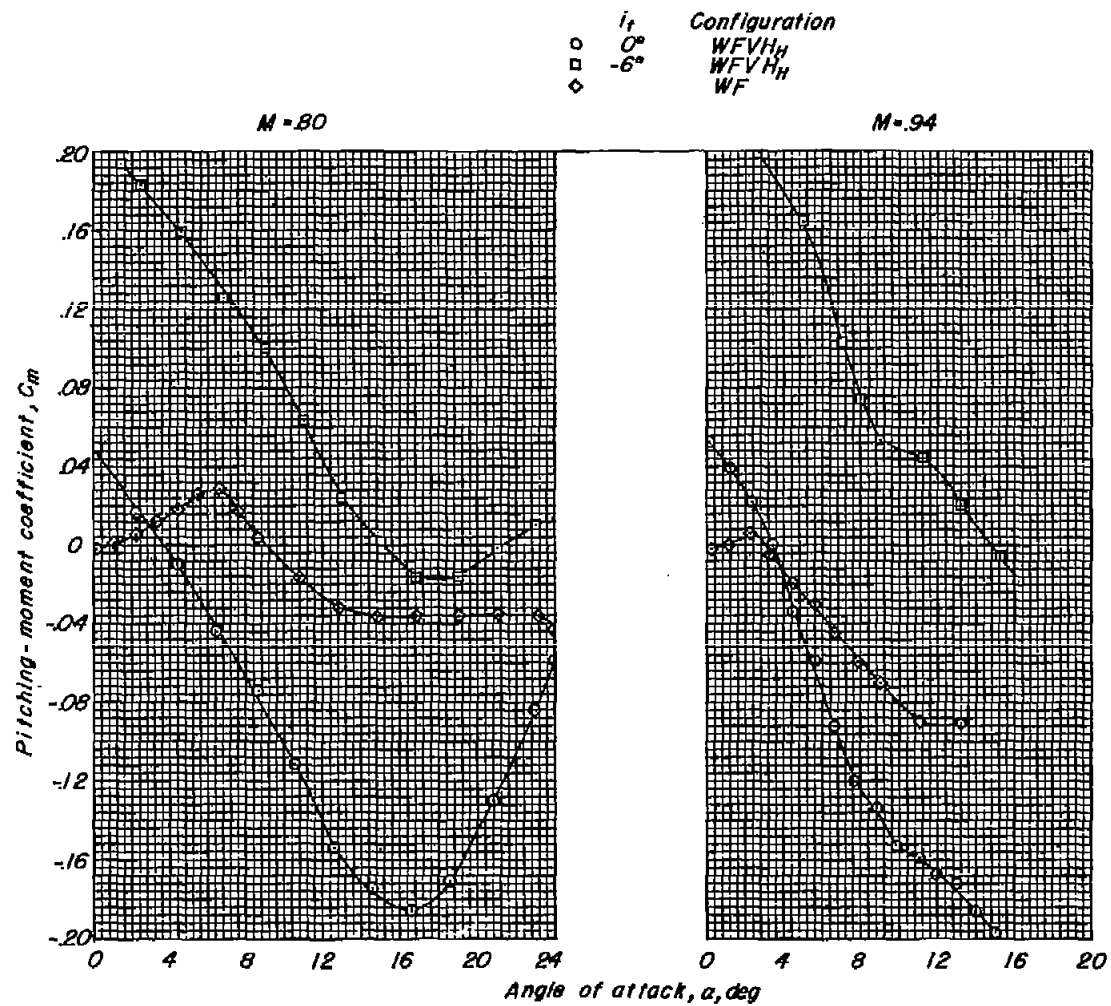
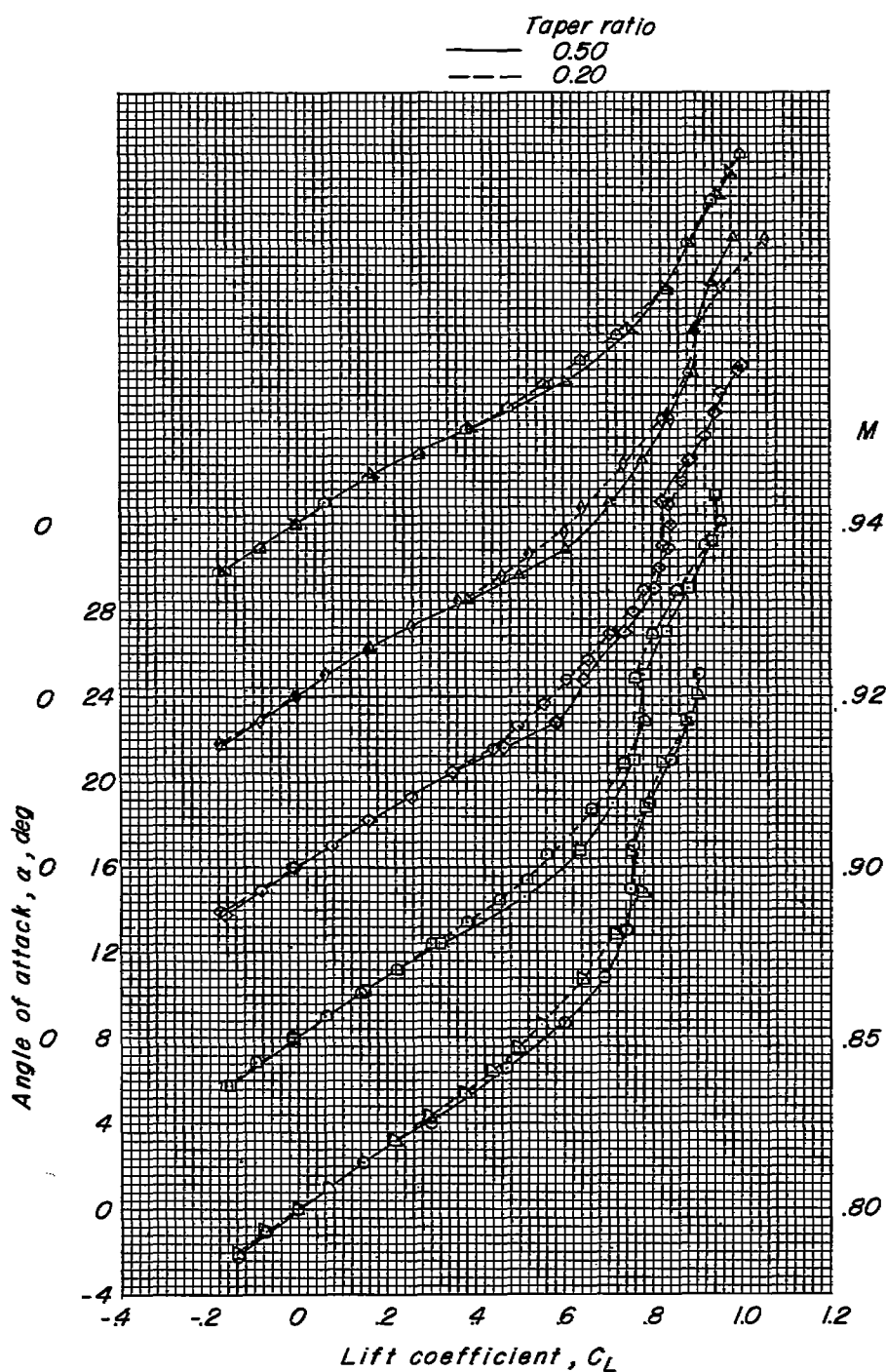
(c) Variation of  $C_m$  with  $\alpha$ ;  $i_t = 0^\circ$ .

Figure 7.- Continued.



(a) Effect of horizontal-tail incidence.

Figure 7.- Concluded.



(a) Variation of  $\alpha$  with  $C_L$ .

Figure 8.- Aerodynamic characteristics of wing-fuselage configuration.  
 $\Lambda_{C/4} = 30^\circ$ .

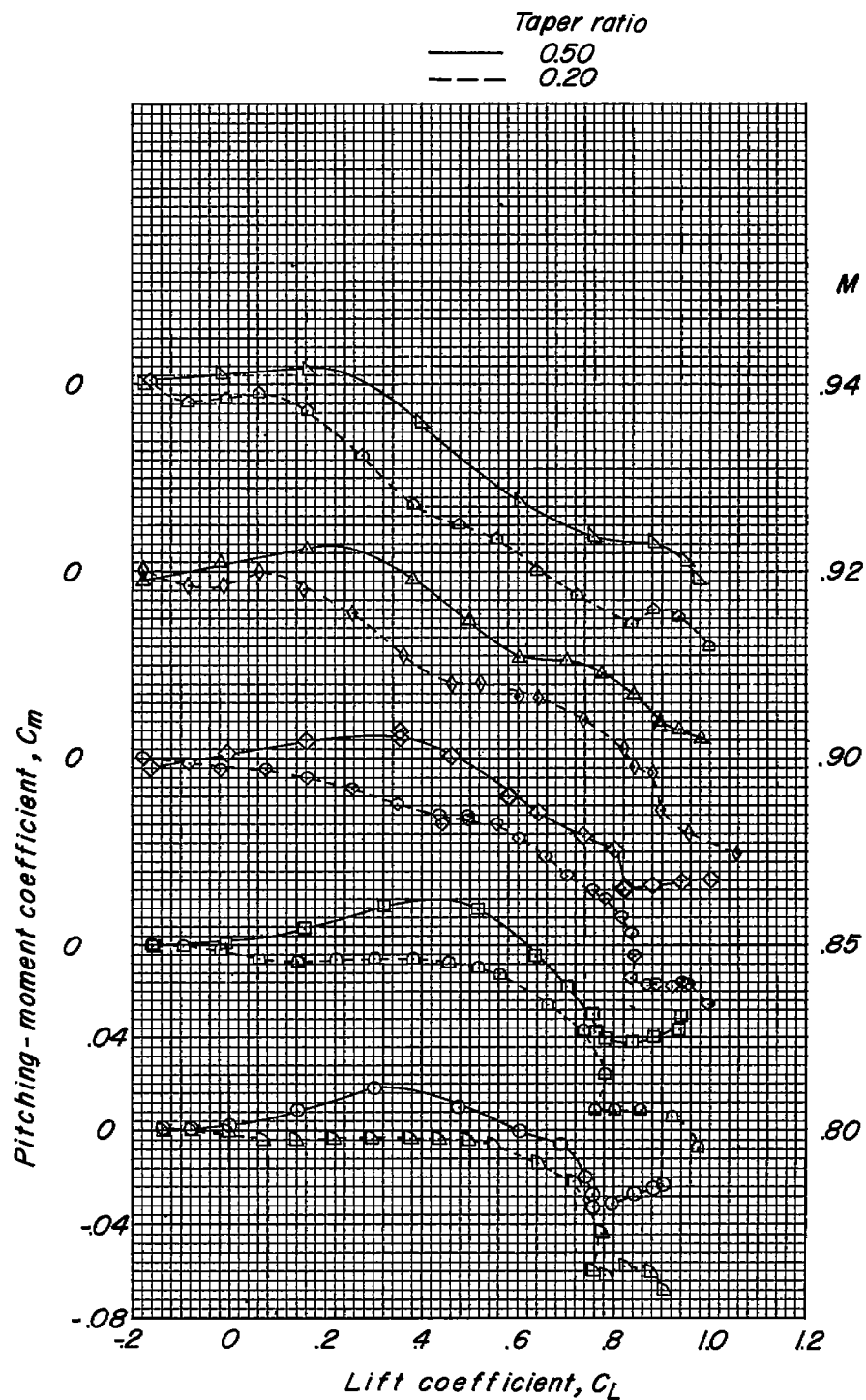
(b) Variation of  $C_m$  with  $C_L$ .

Figure 8.- Continued.

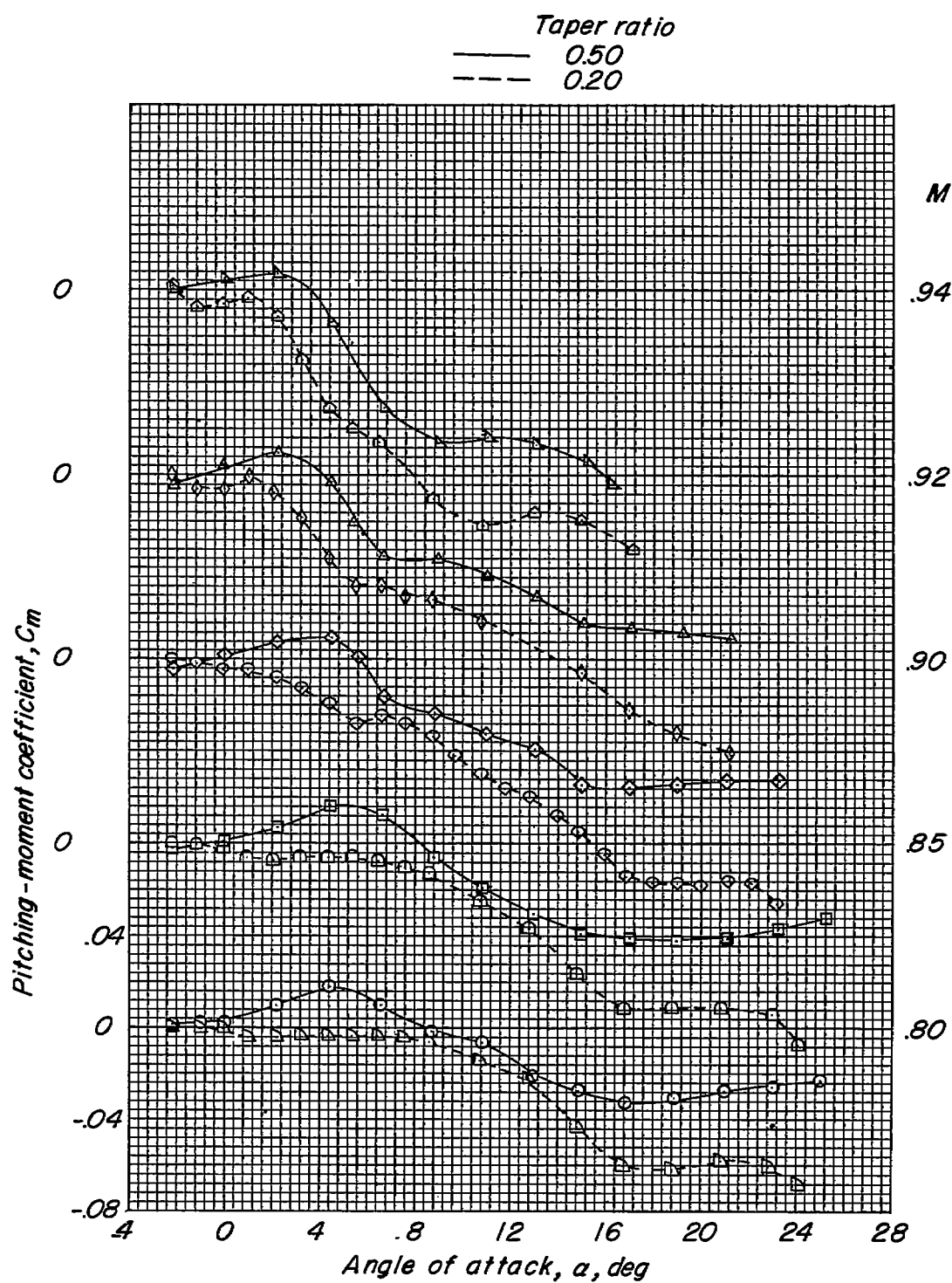
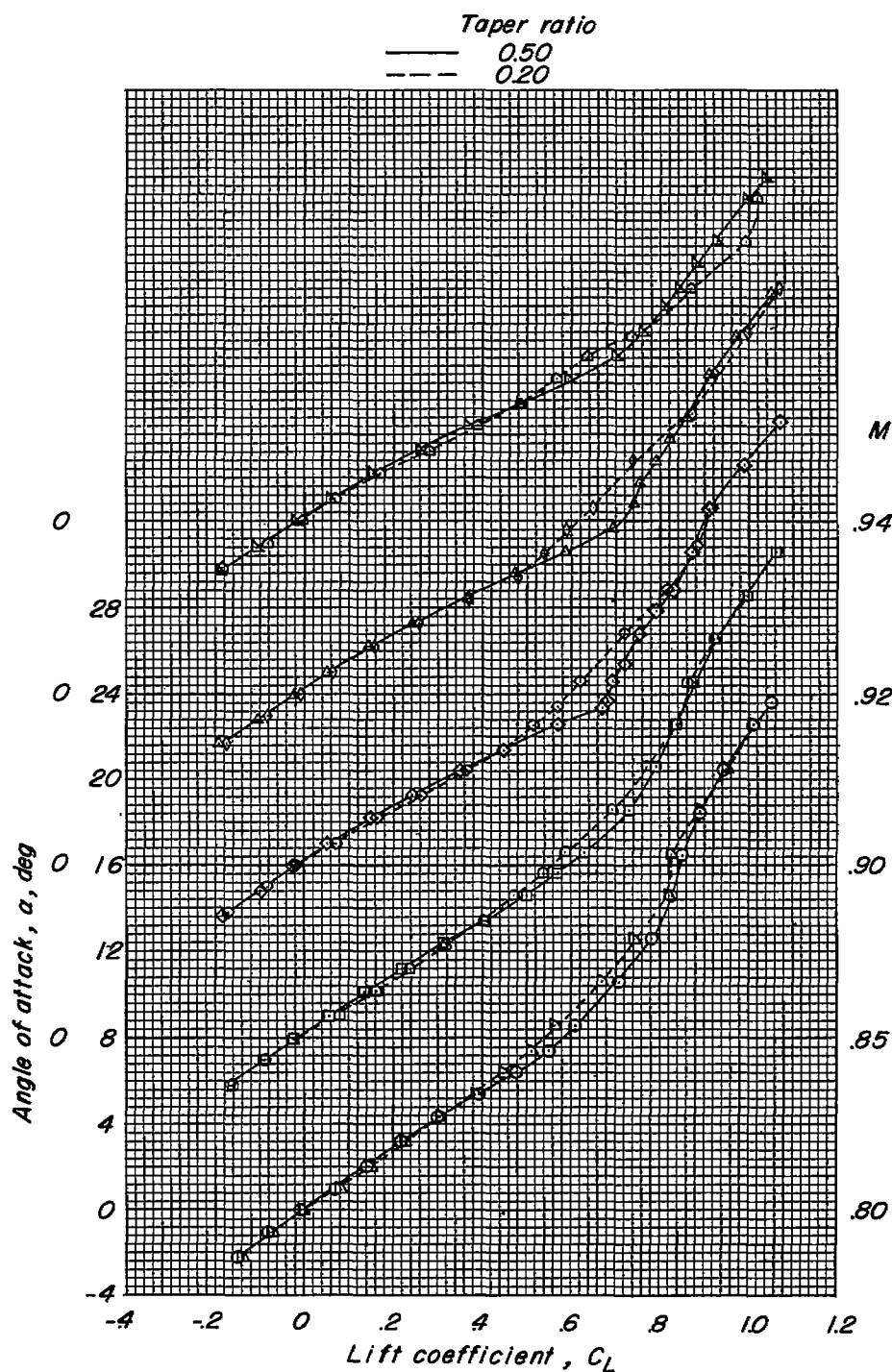
(c) Variation of  $C_m$  with  $\alpha$ .

Figure 8.- Concluded.



(a) Variation of  $\alpha$  with  $C_L$ .

Figure 9.- Aerodynamic characteristics of a wing-fuselage-low-tail configuration.  $\Lambda_c/4 = 30^\circ$ ;  $i_t = 0^\circ$ .

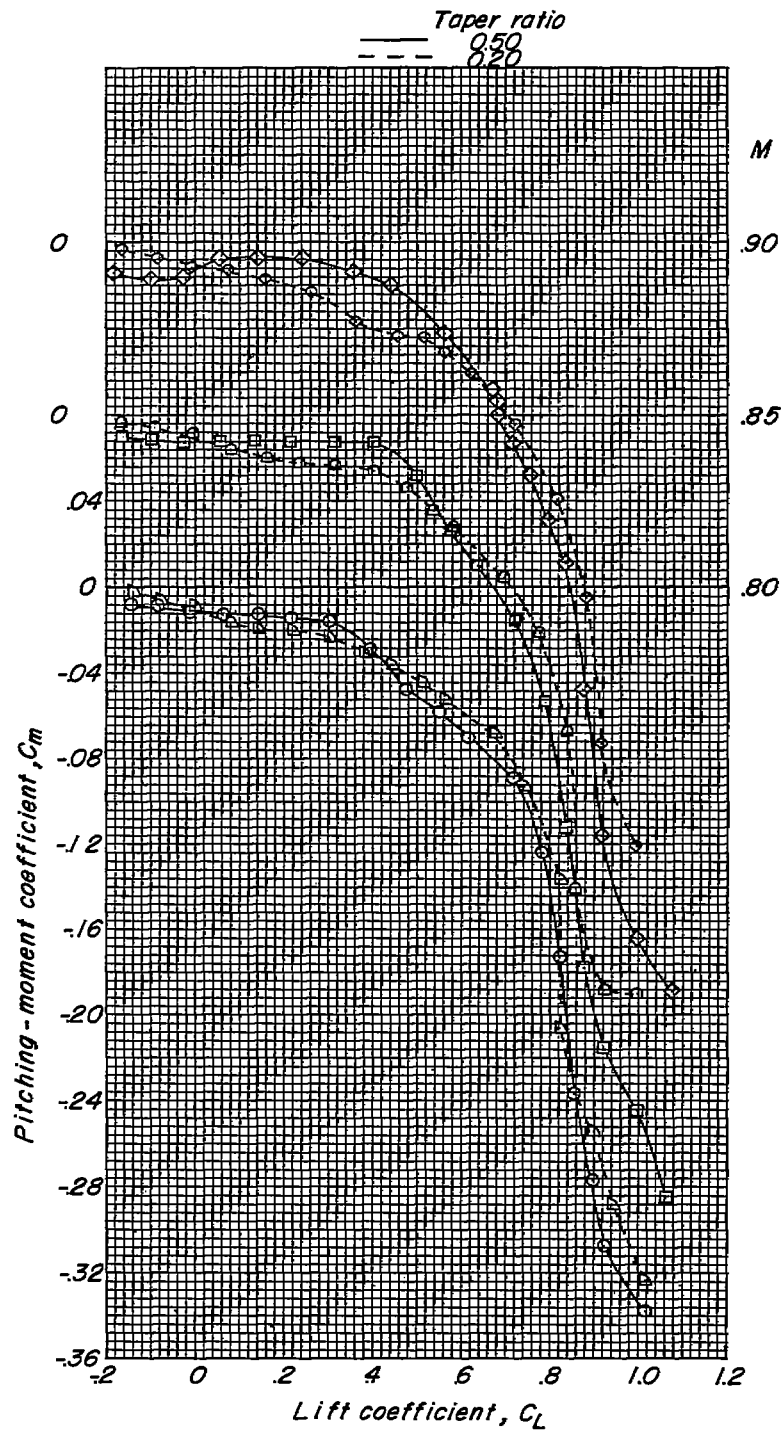
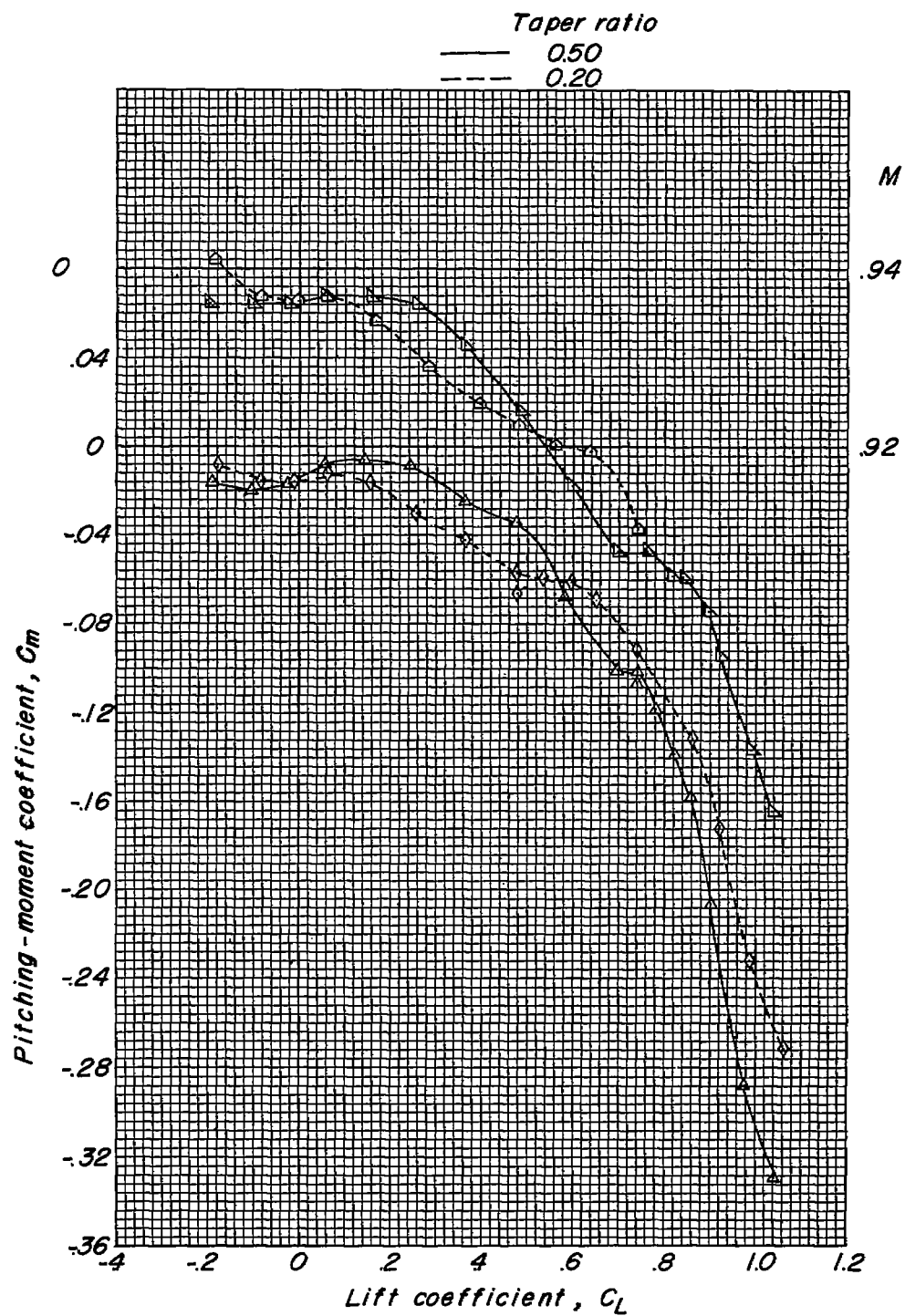
(b) Variation of  $C_m$  with  $C_L$ .

Figure 9.- Continued.



(b) Concluded.

Figure 9.- Continued.

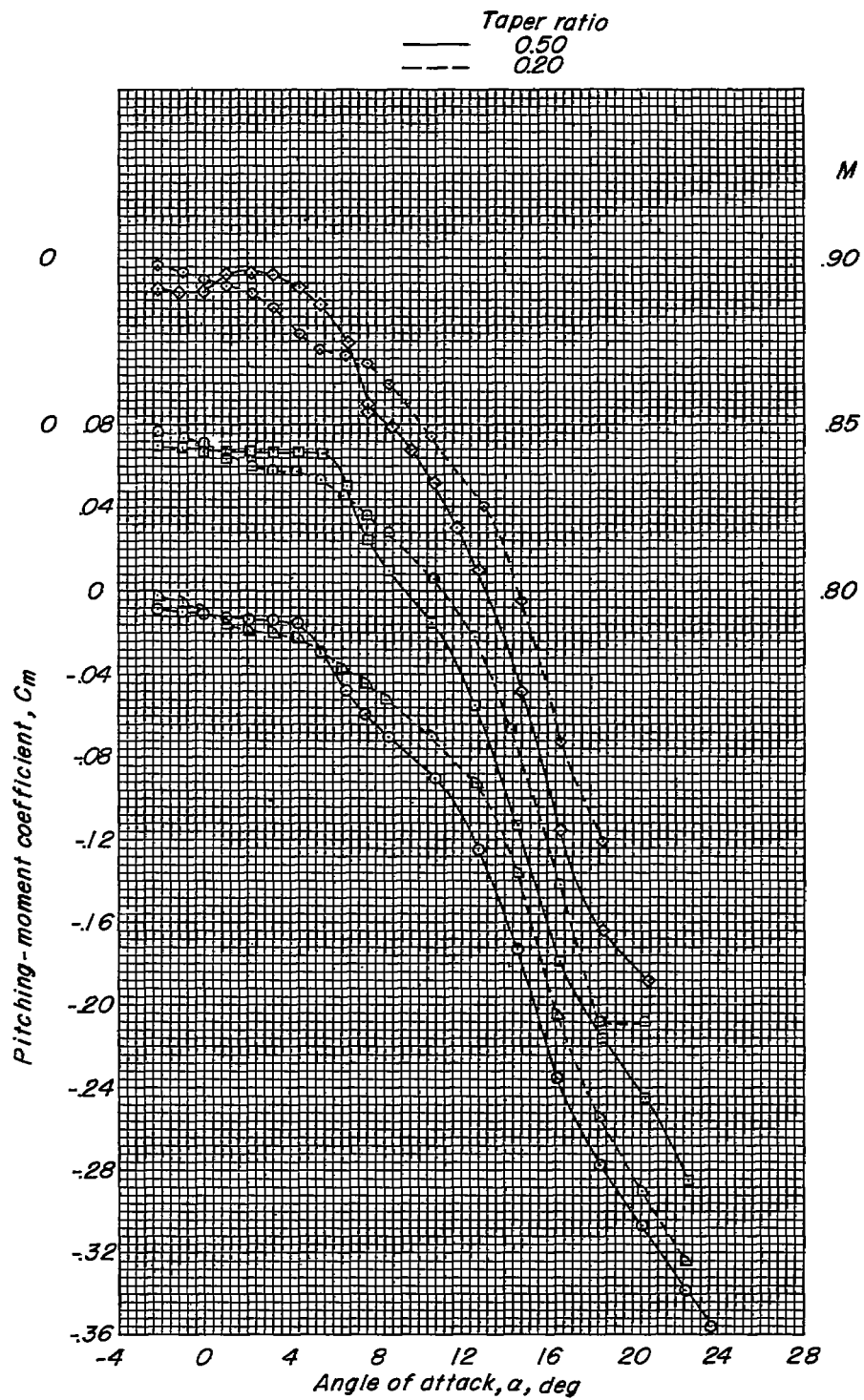
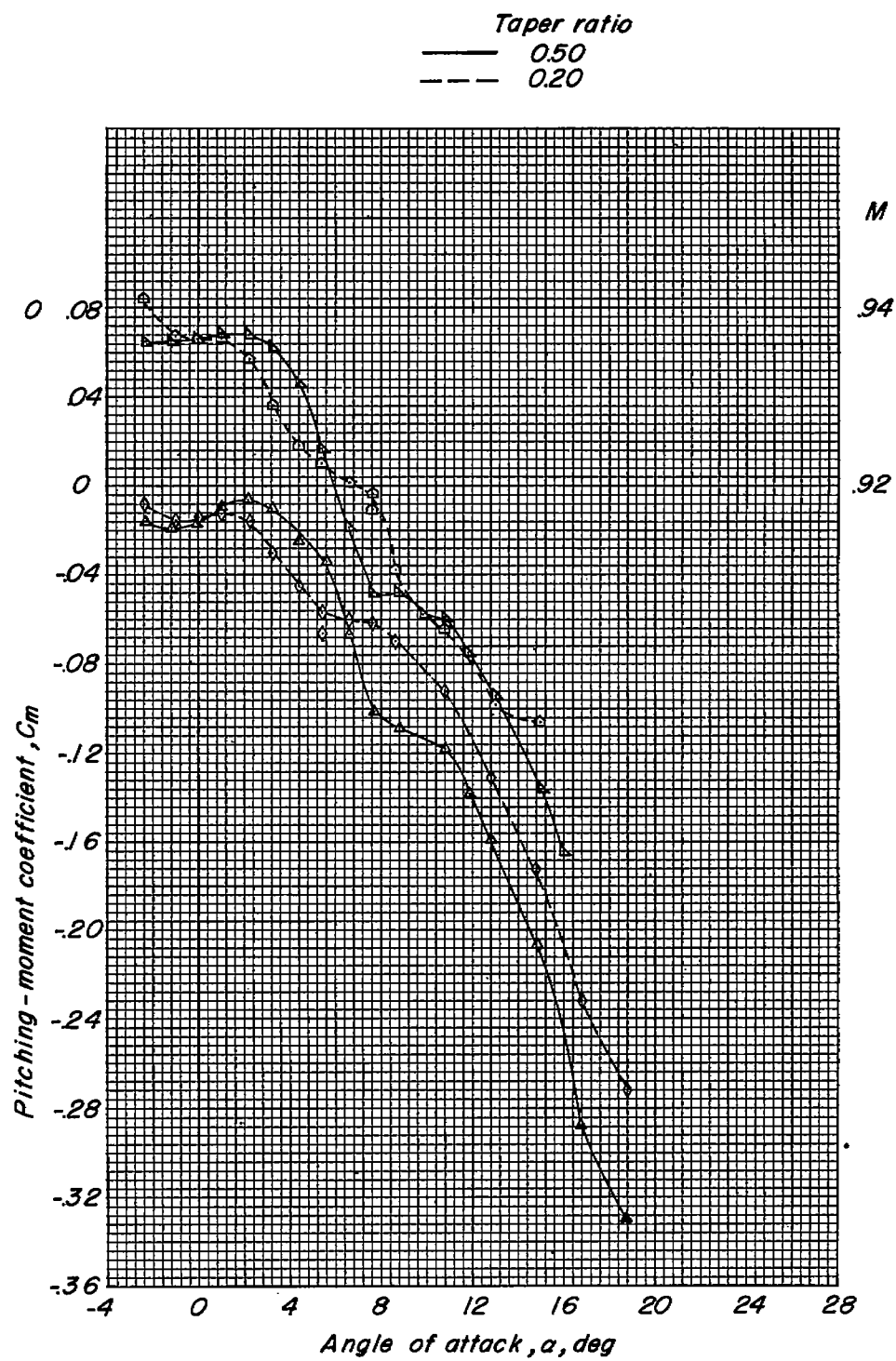
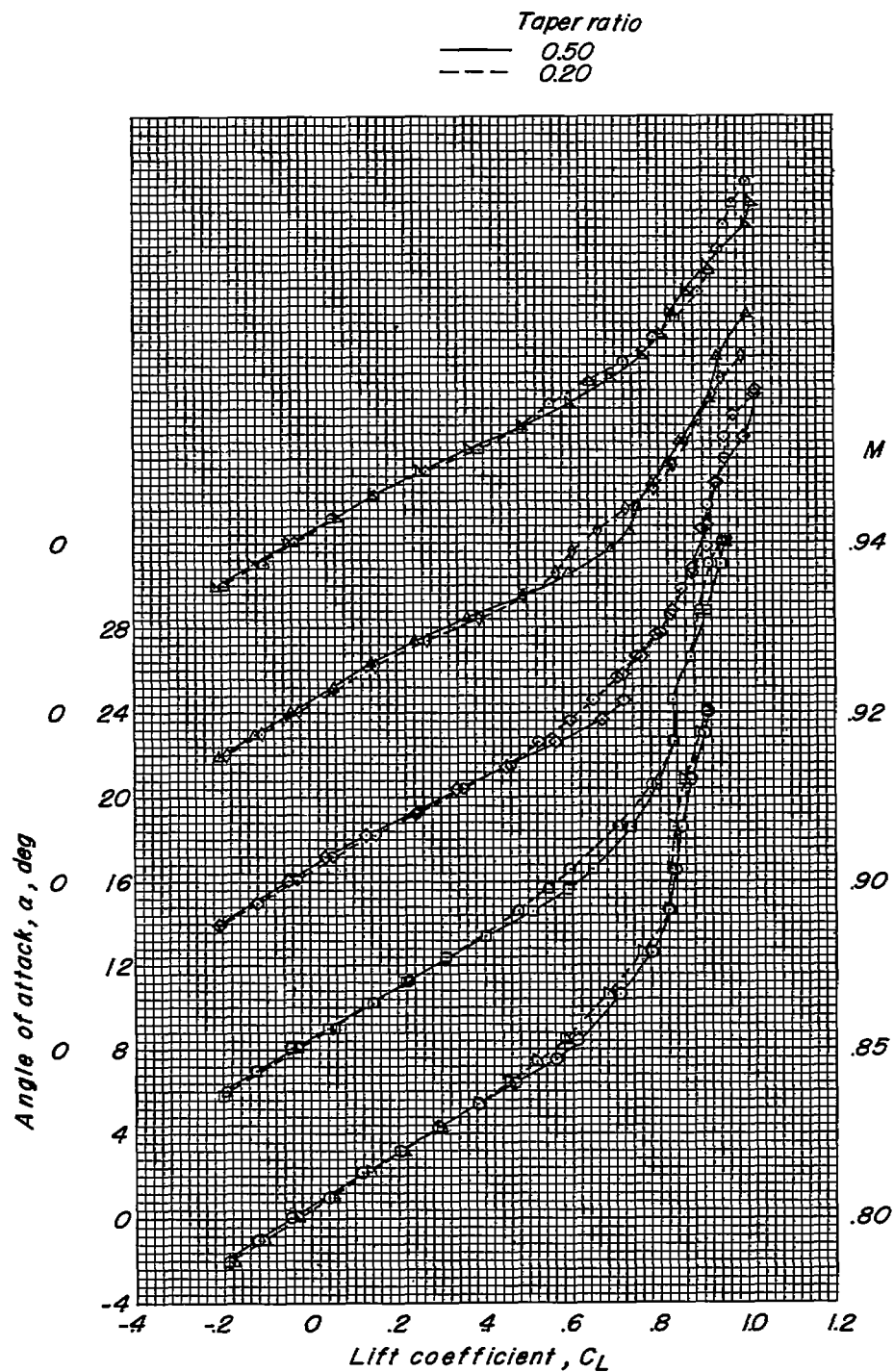
(c) Variation of  $C_m$  with  $\alpha$ .

Figure 9.- Continued.



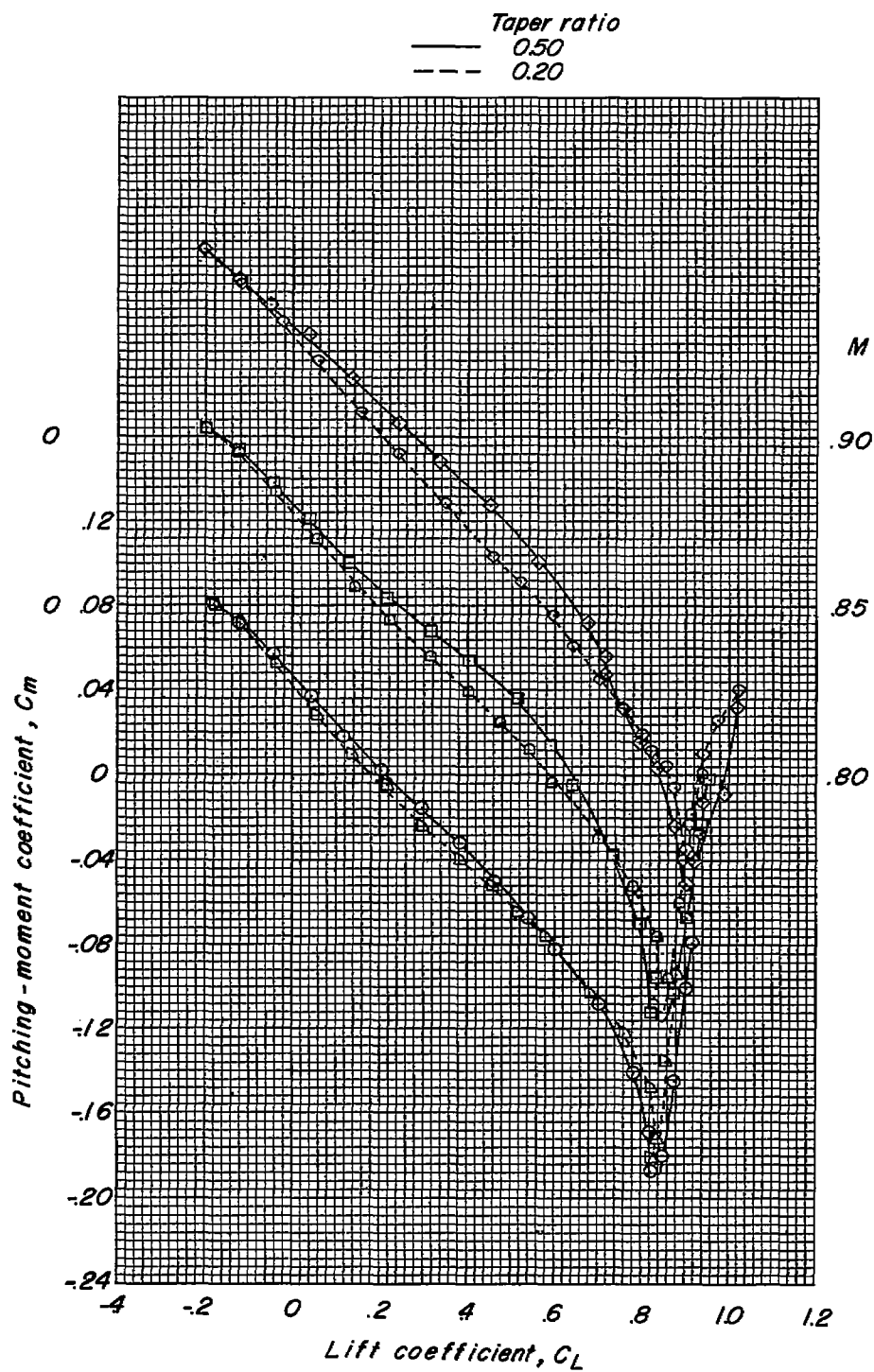
(c) Concluded.

Figure 9.- Concluded.



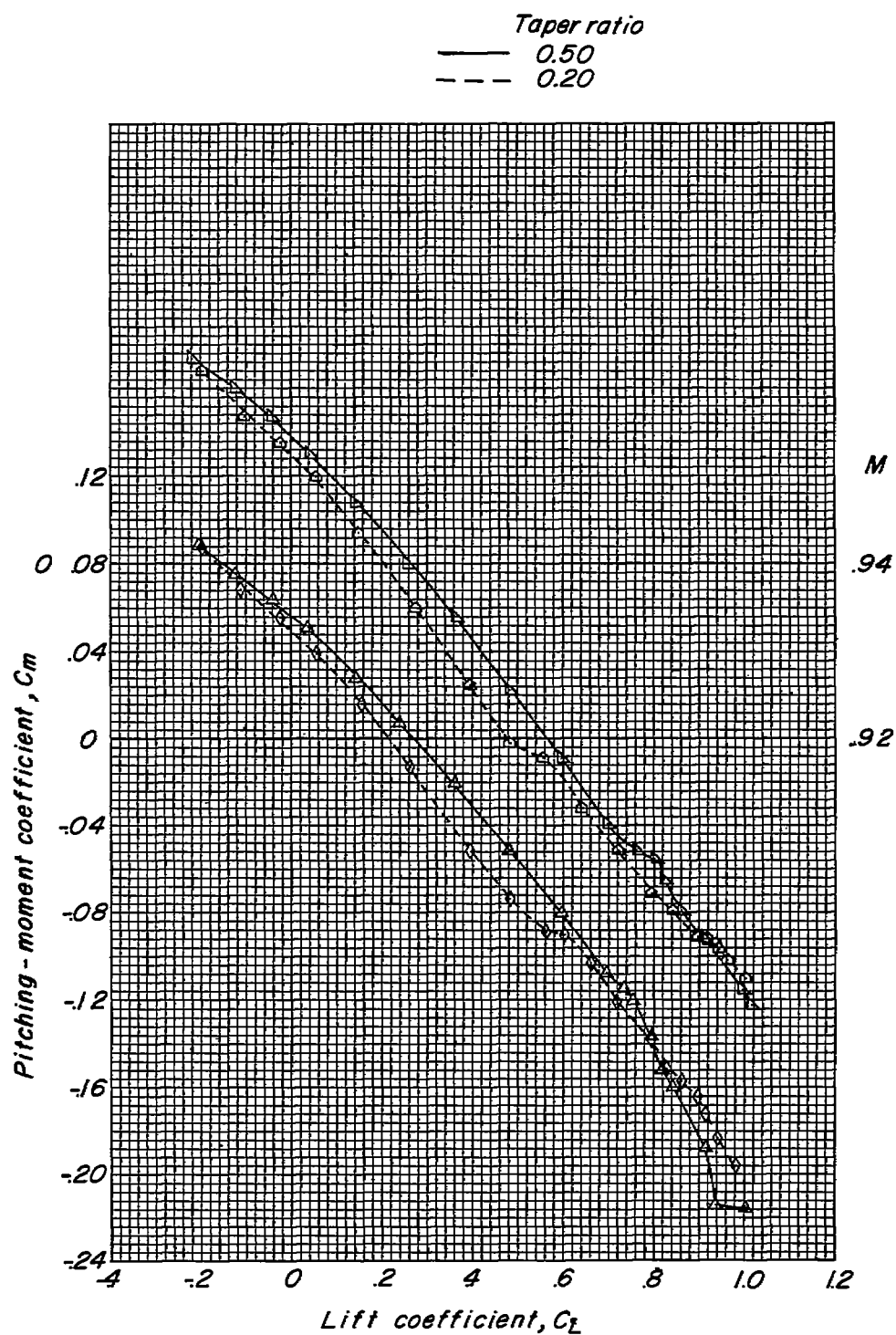
(a) Variation of  $\alpha$  with  $C_L$ ;  $i_t = 0^\circ$ .

Figure 10.- Aerodynamic characteristics of wing-fuselage-high-tail configuration.  $\Lambda_{C/4} = 30^\circ$ .



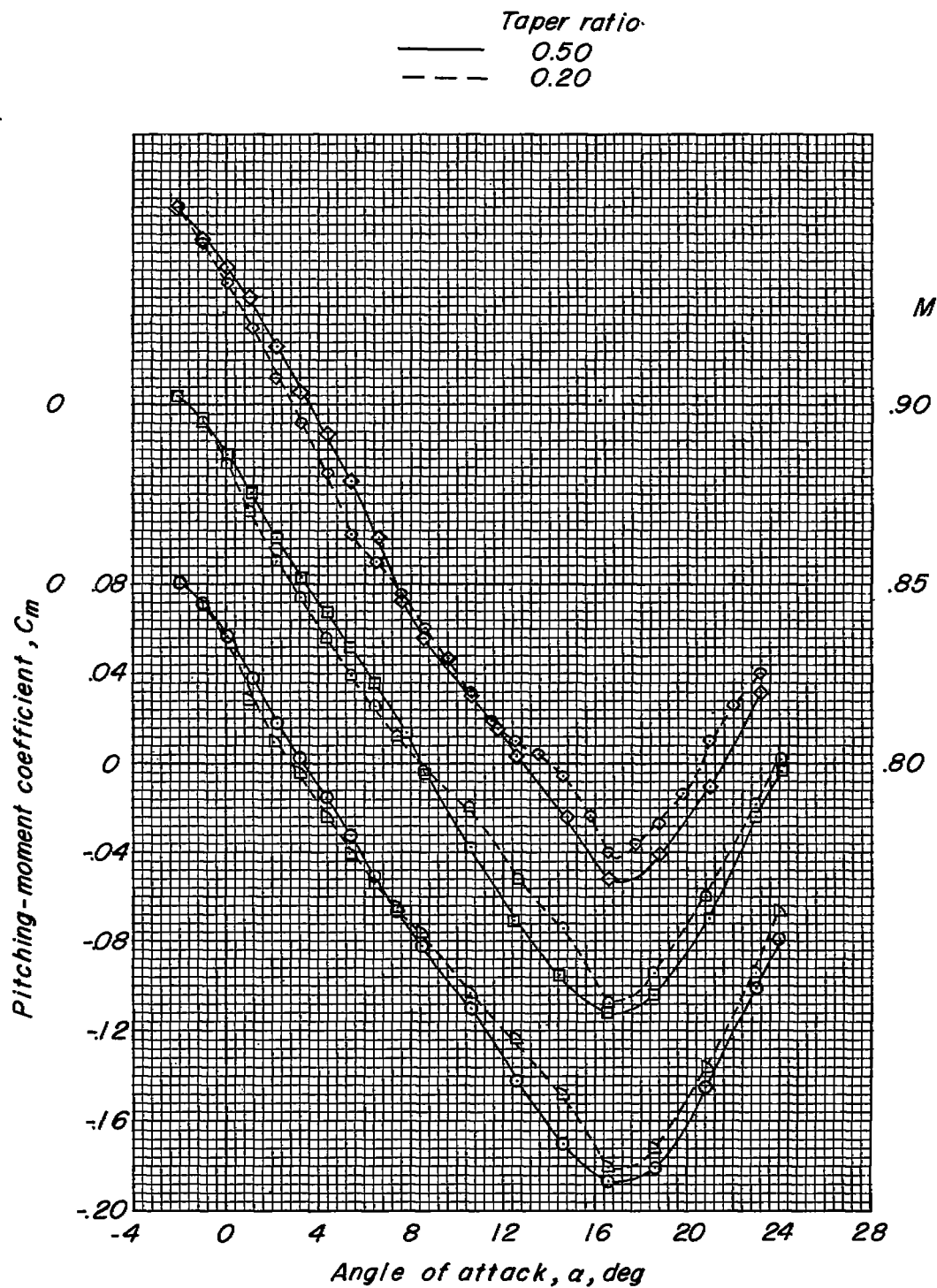
(b) Variation of  $C_m$  with  $C_L$ ;  $i_t = 0^\circ$ .

Figure 10.- Continued.



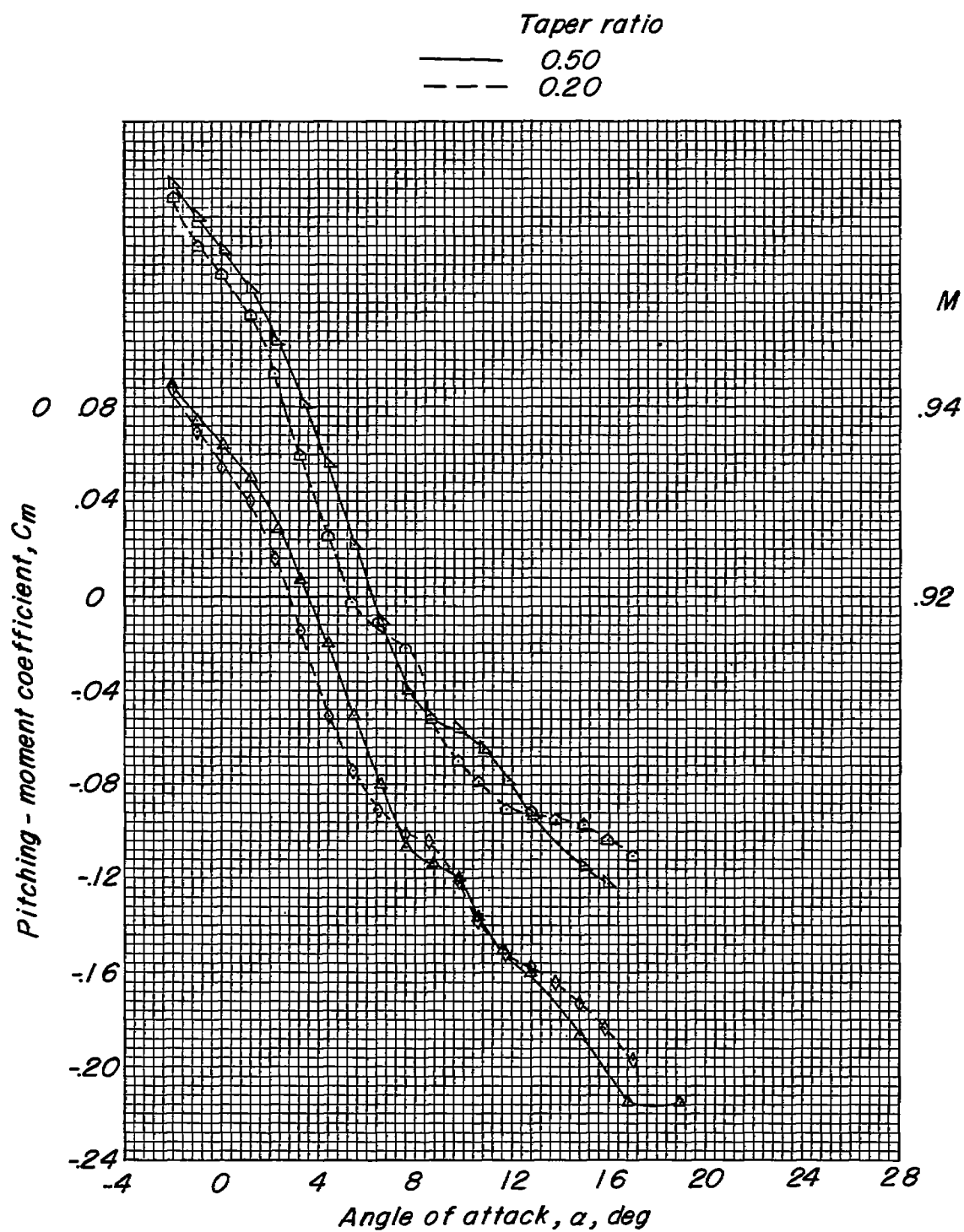
(b) Concluded.

Figure 10.- Continued.



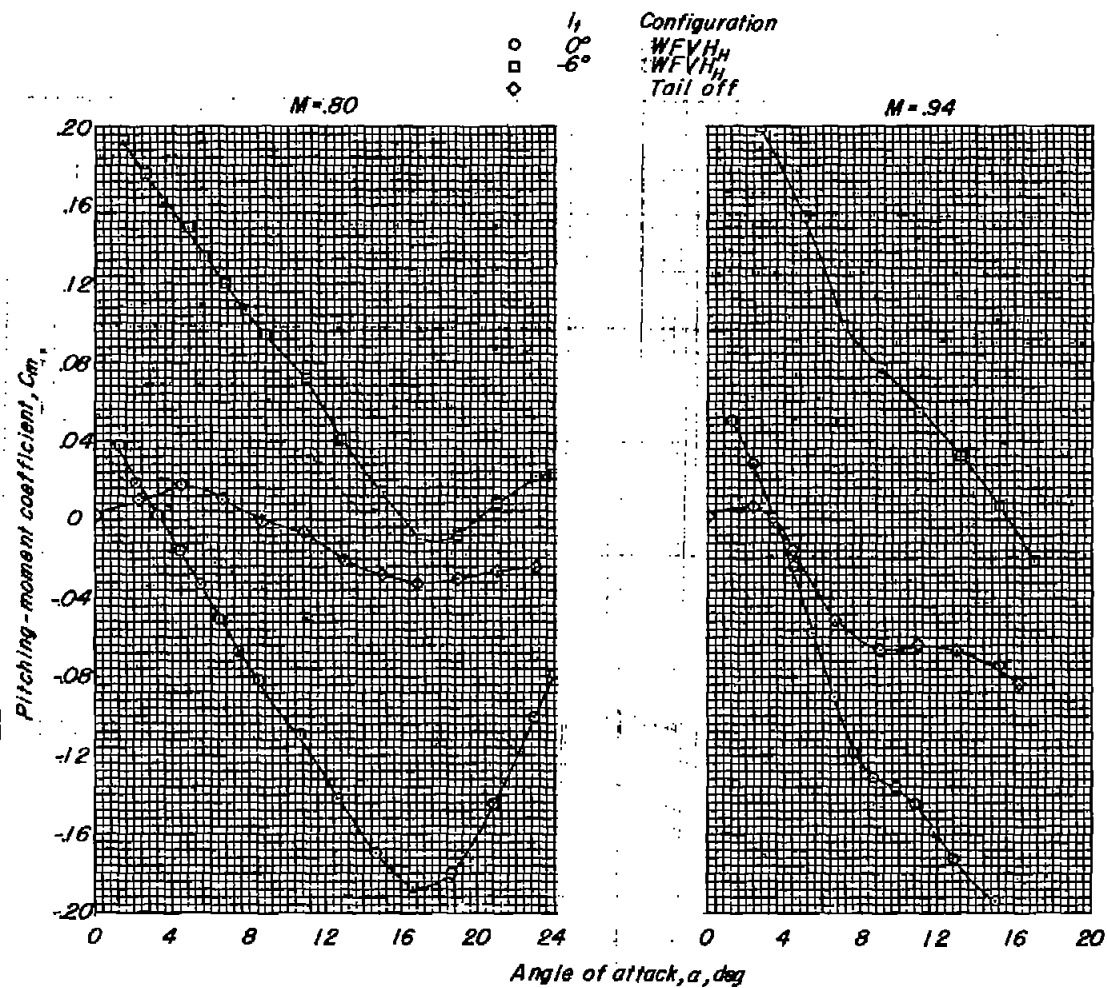
(c) Variation of  $C_m$  with  $\alpha$ ;  $i_t = 0^\circ$ .

Figure 10.- Continued.



(c) Concluded.

Figure 10.- Continued.



(d) Effect of horizontal-tail incidence.

Figure 10.- Concluded.

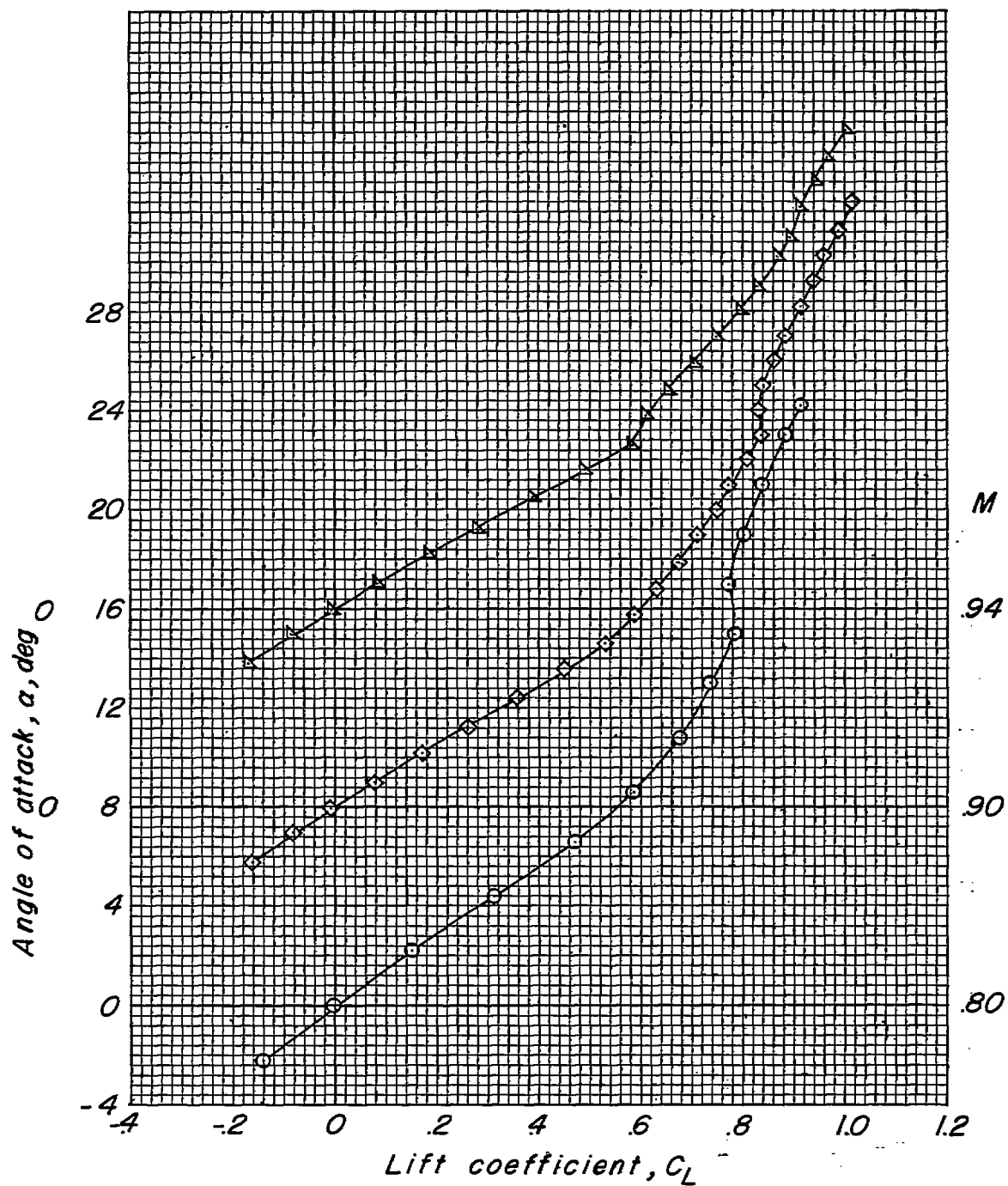
(a) Variation of  $\alpha$  with  $C_L$ .

Figure 11.- Aerodynamic characteristics of wing-fuselage configuration.  
 $\Lambda_{c/4} = 35^\circ$ ;  $\lambda = 0.50$ .

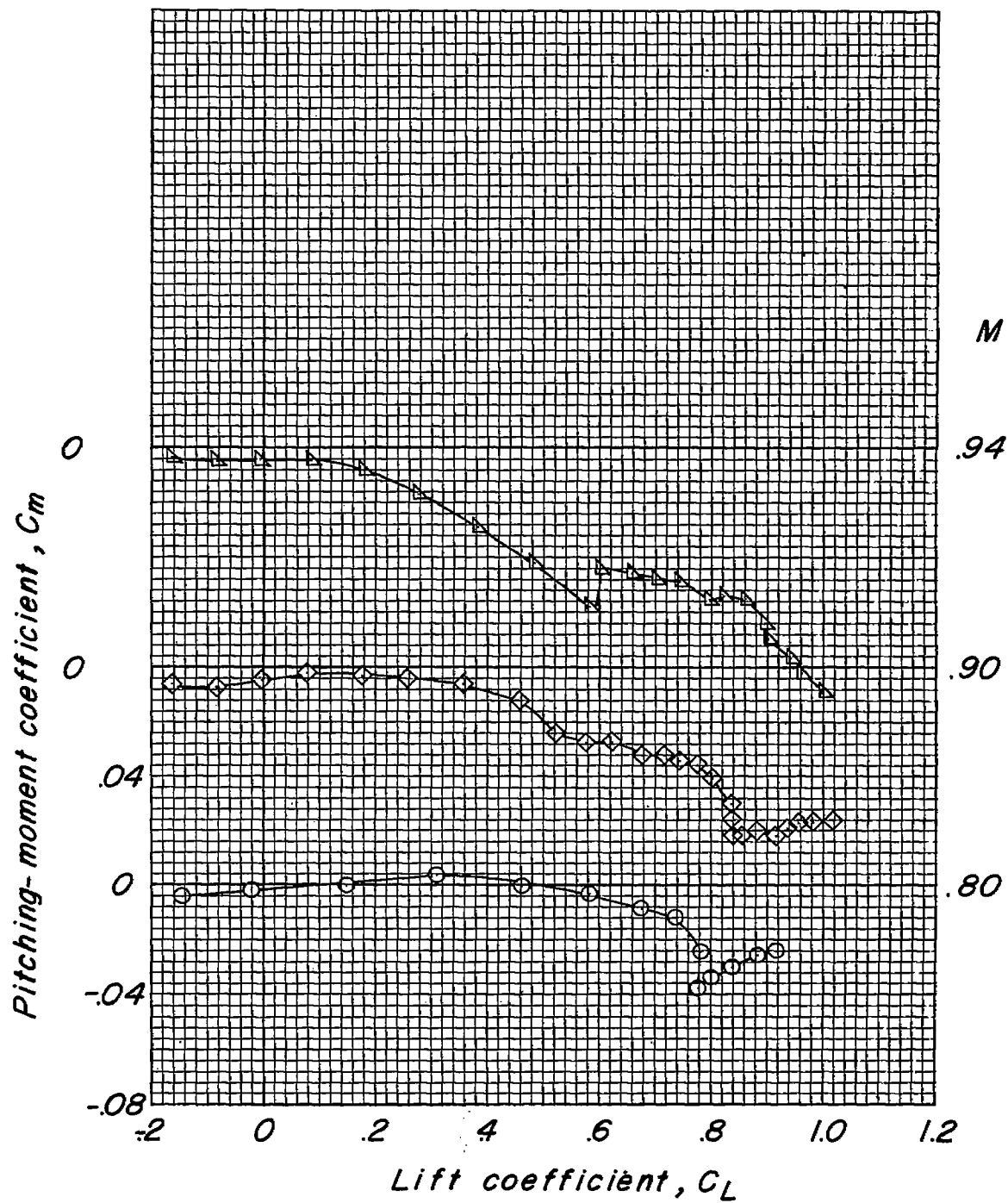
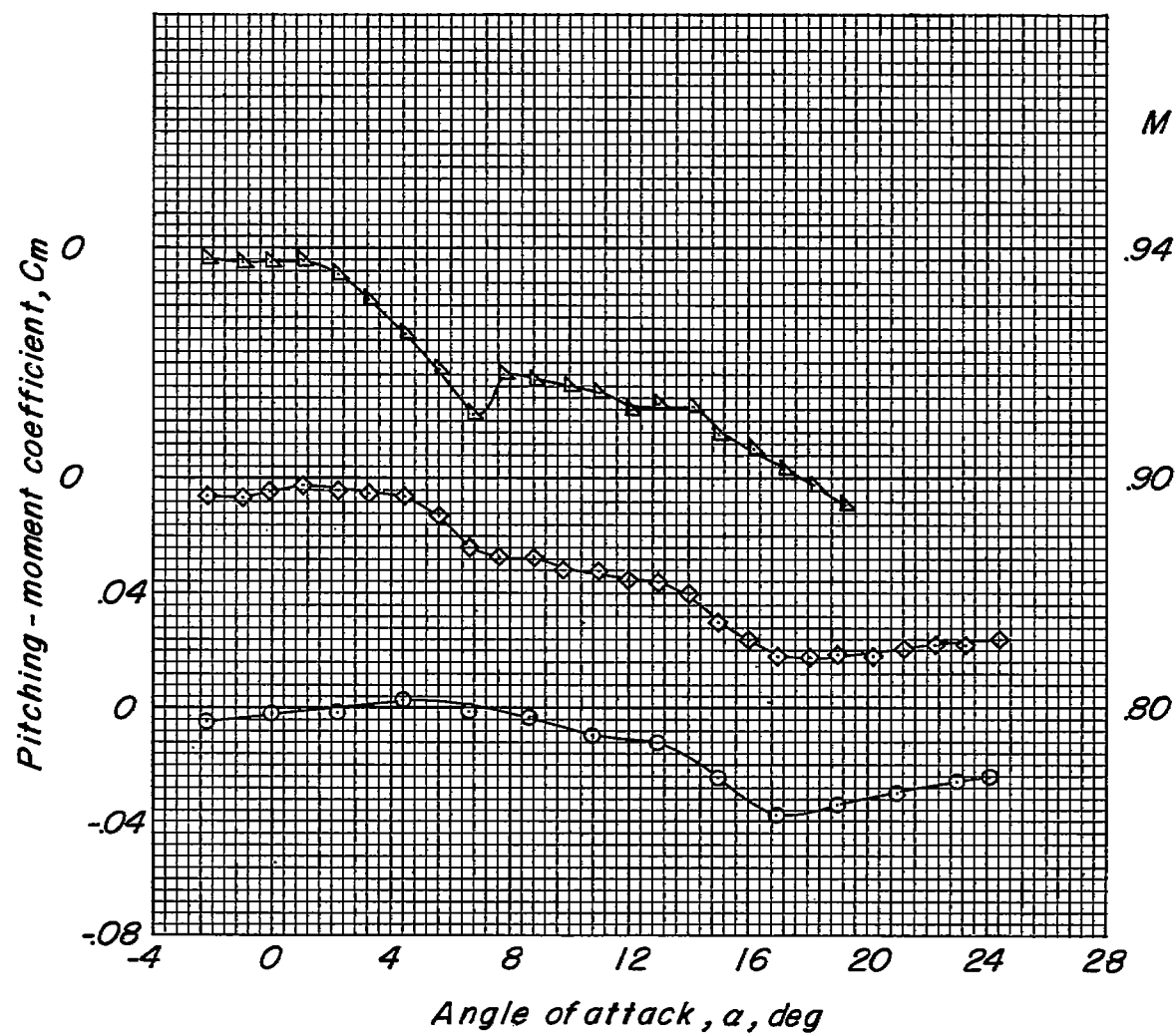
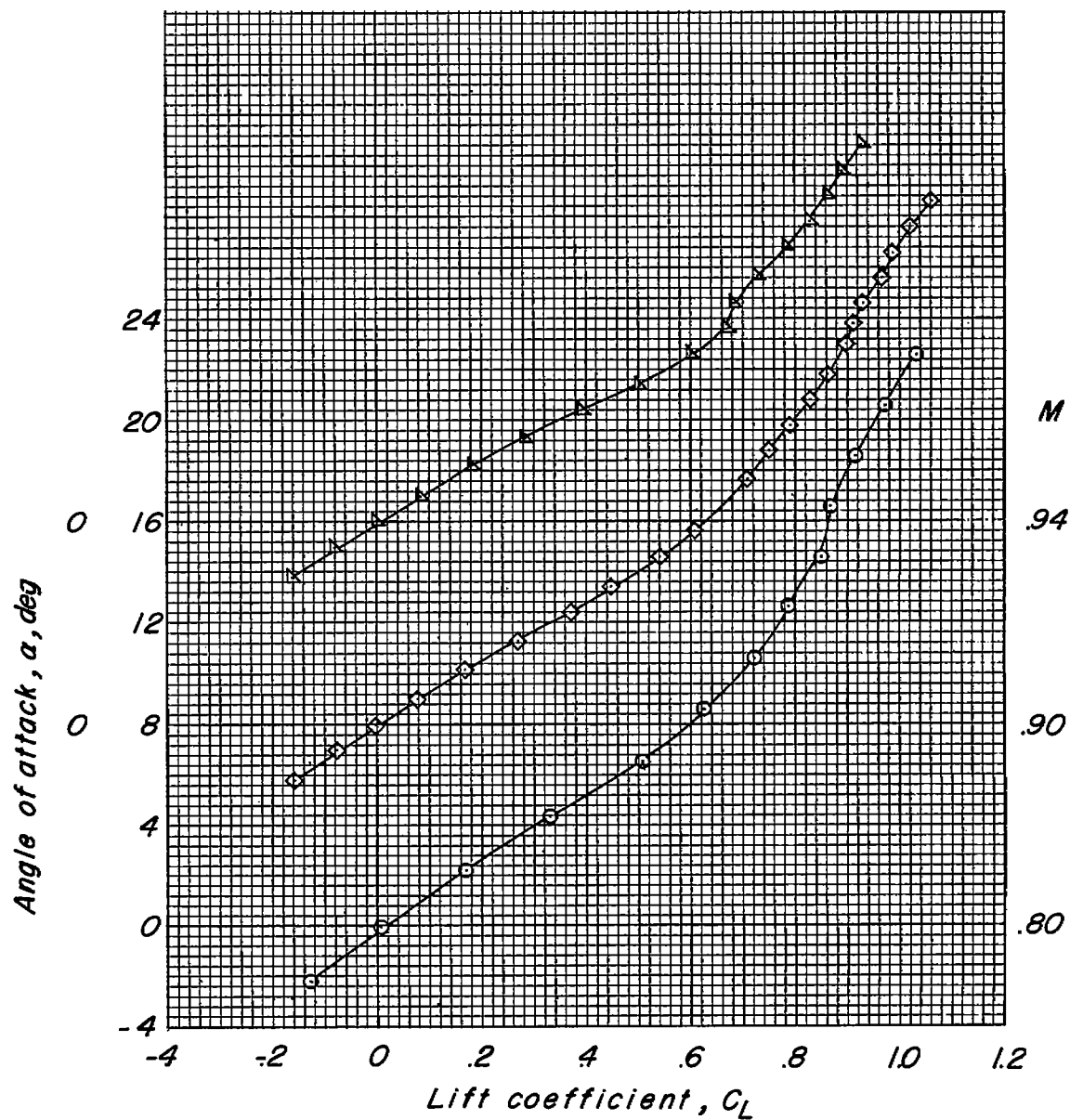
(b) Variation of  $C_m$  with  $C_L$ .

Figure 11.- Continued.



(c) Variation of  $C_m$  with  $\alpha$ .

Figure 11.- Concluded.



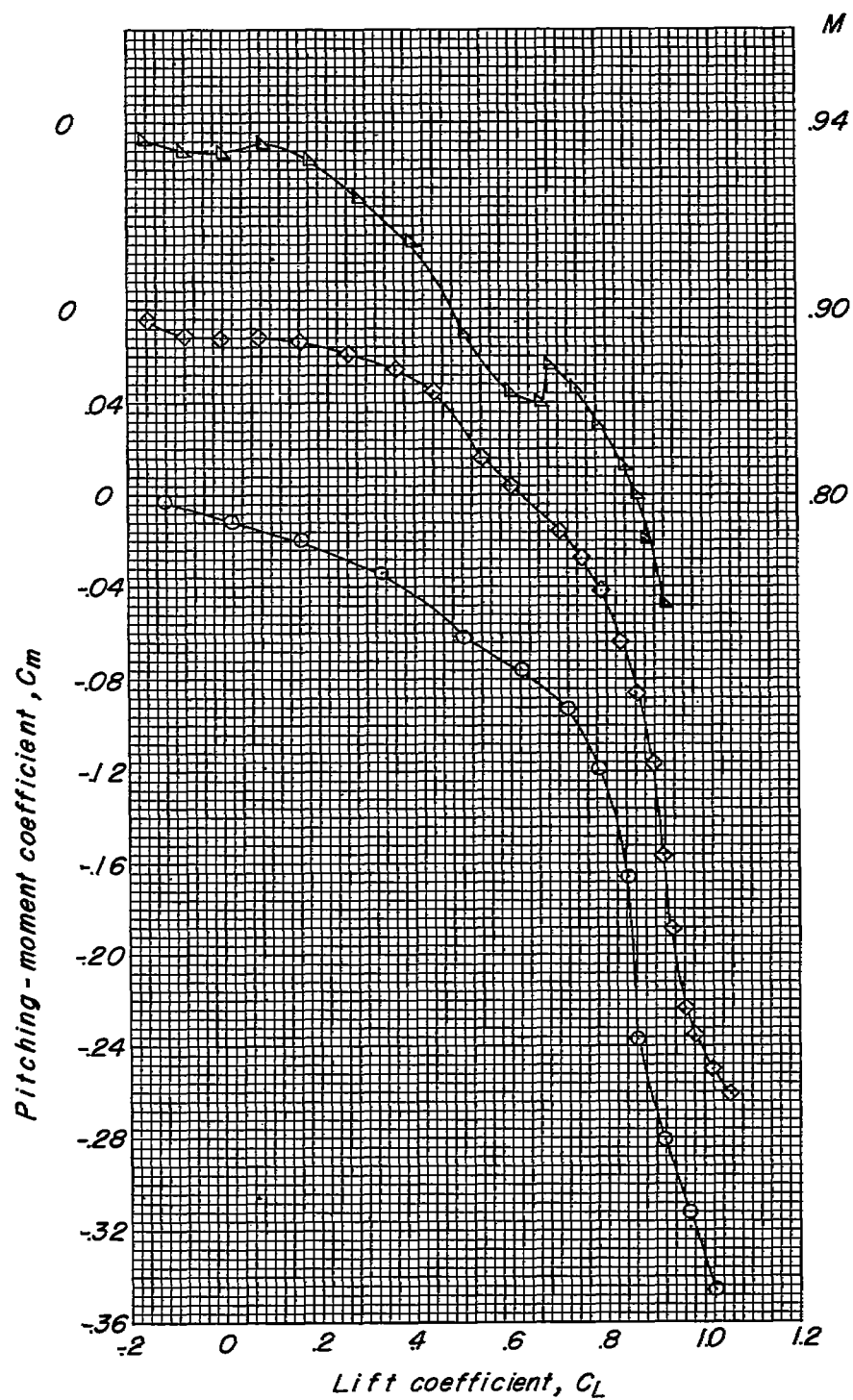
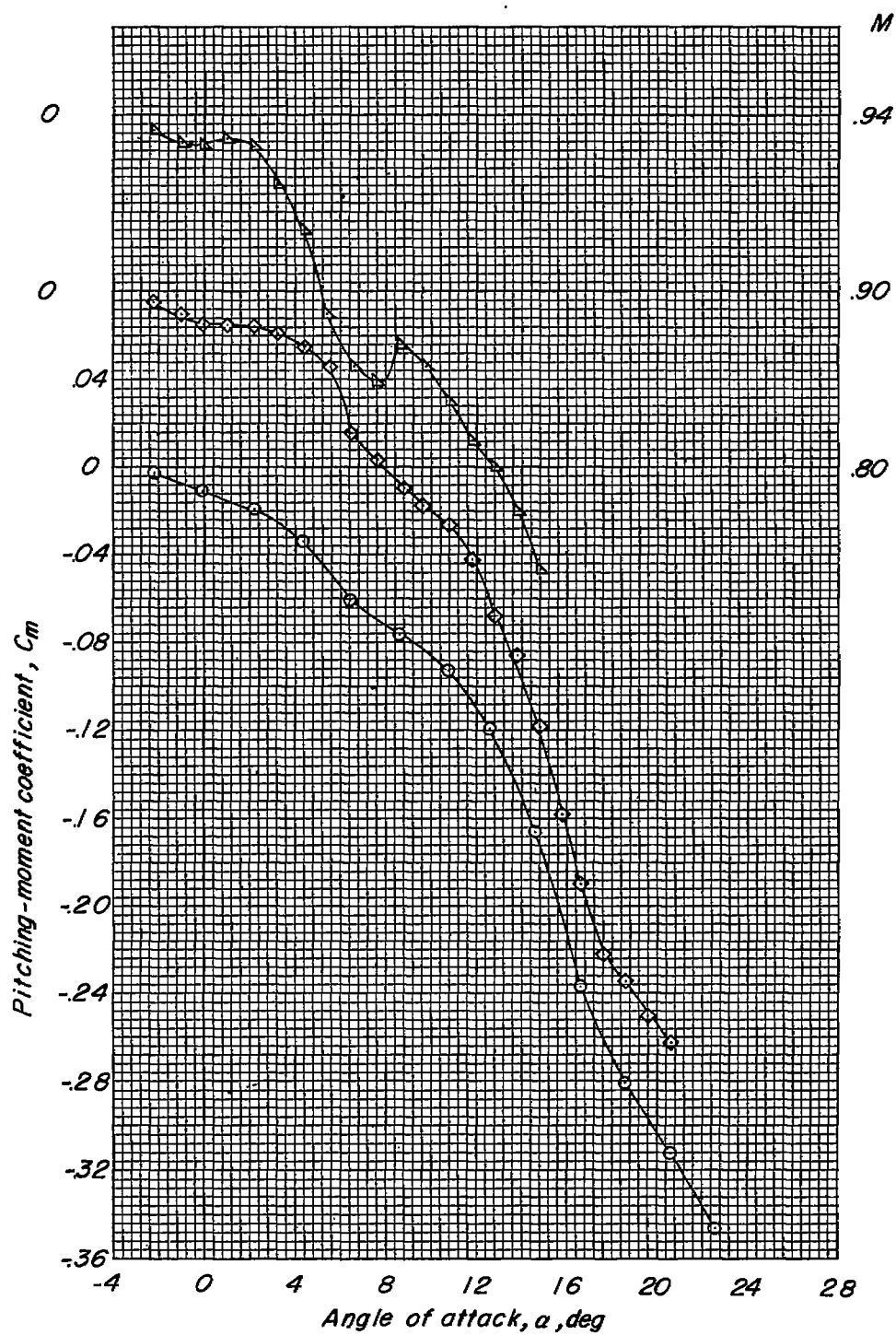
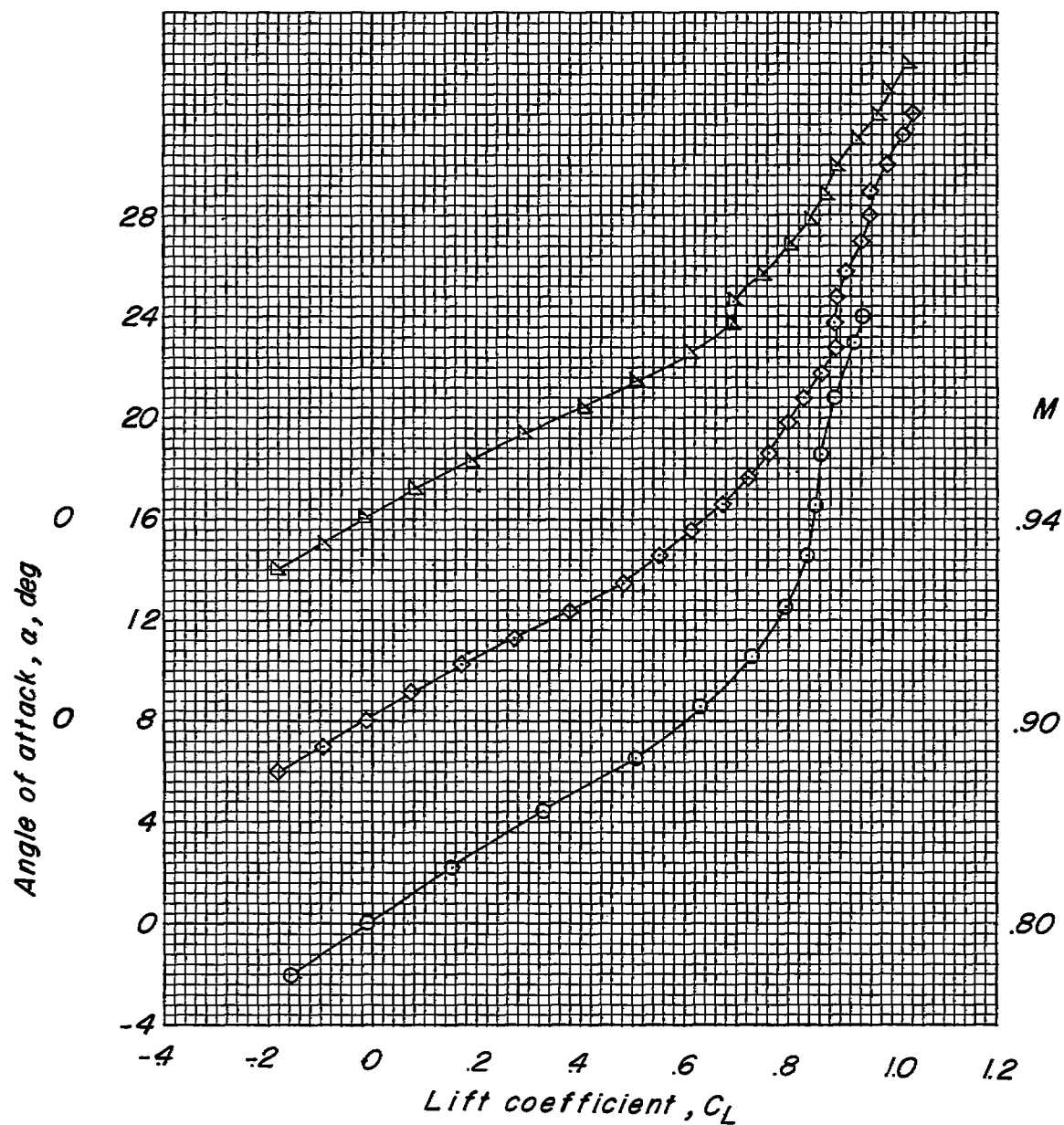
(b) Variation of  $C_m$  with  $C_L$ .

Figure 12.- Continued.



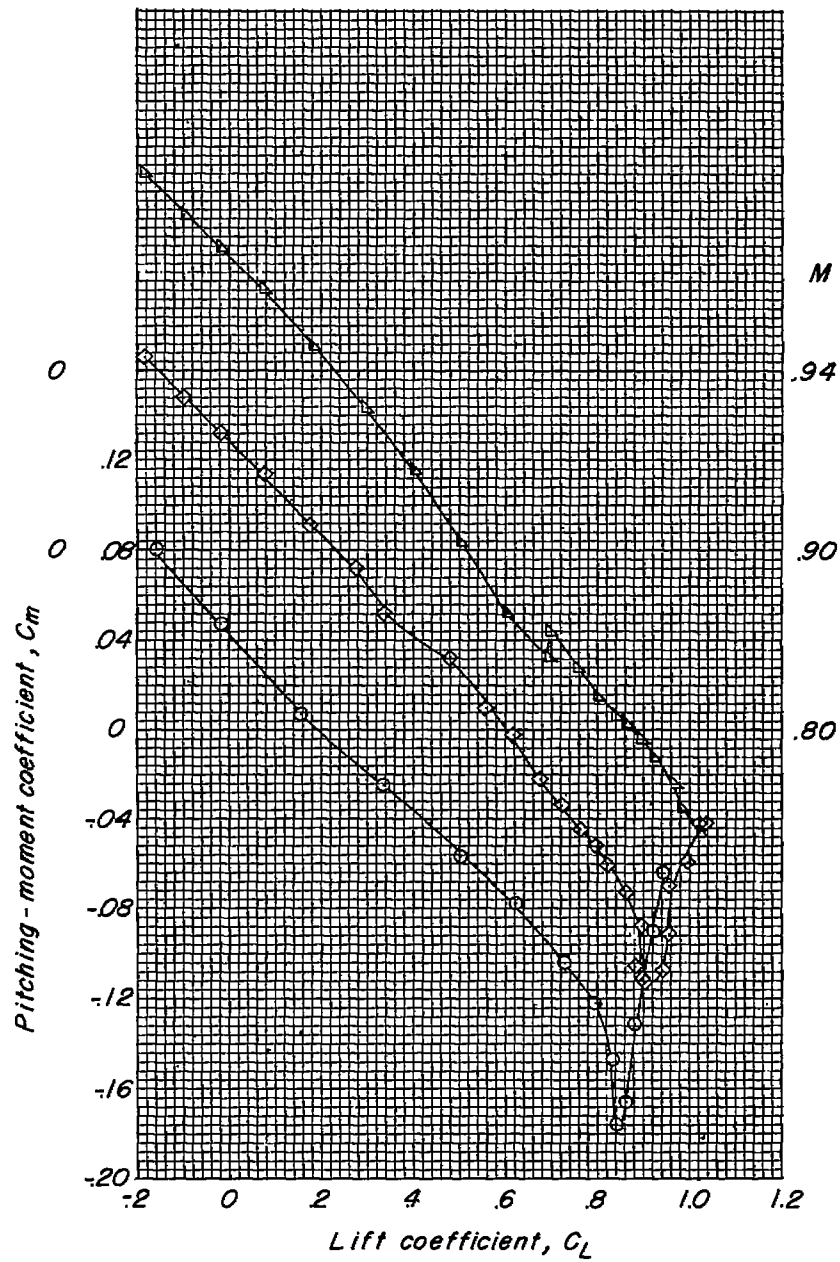
(c) Variation of  $C_m$  with  $\alpha$ .

Figure 12.- Concluded.



(a) Variation of  $\alpha$  with  $C_L$ ;  $i_t = 0^\circ$ .

Figure 13.- Aerodynamic characteristics of wing-fuselage-high-tail configuration.  $\Lambda_c/4 = 35^\circ$ ;  $\lambda = 0.50$ .



(b) Variation of  $C_m$  with  $C_L$ ;  $i_t = 0^\circ$ .

Figure 13.- Continued.

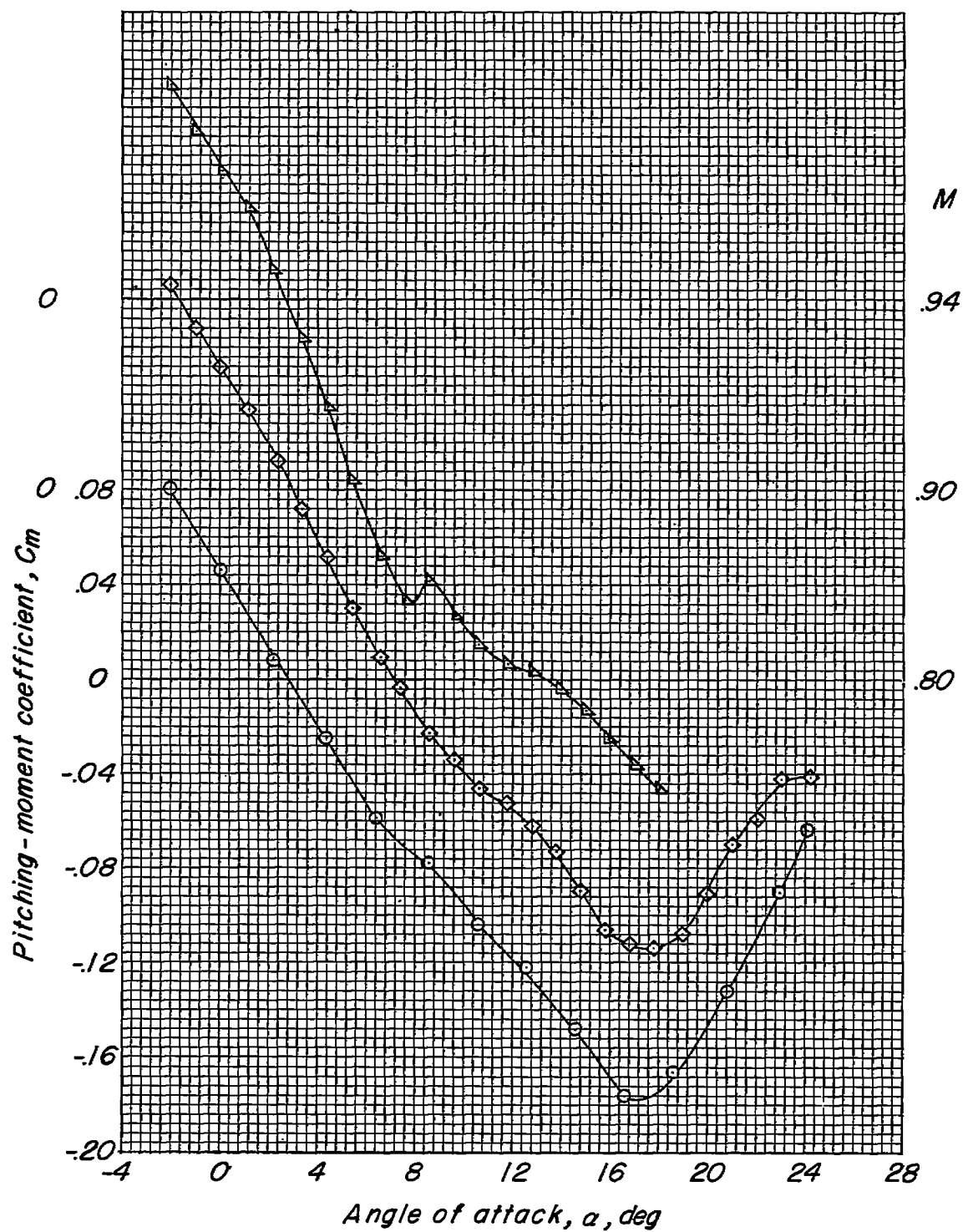
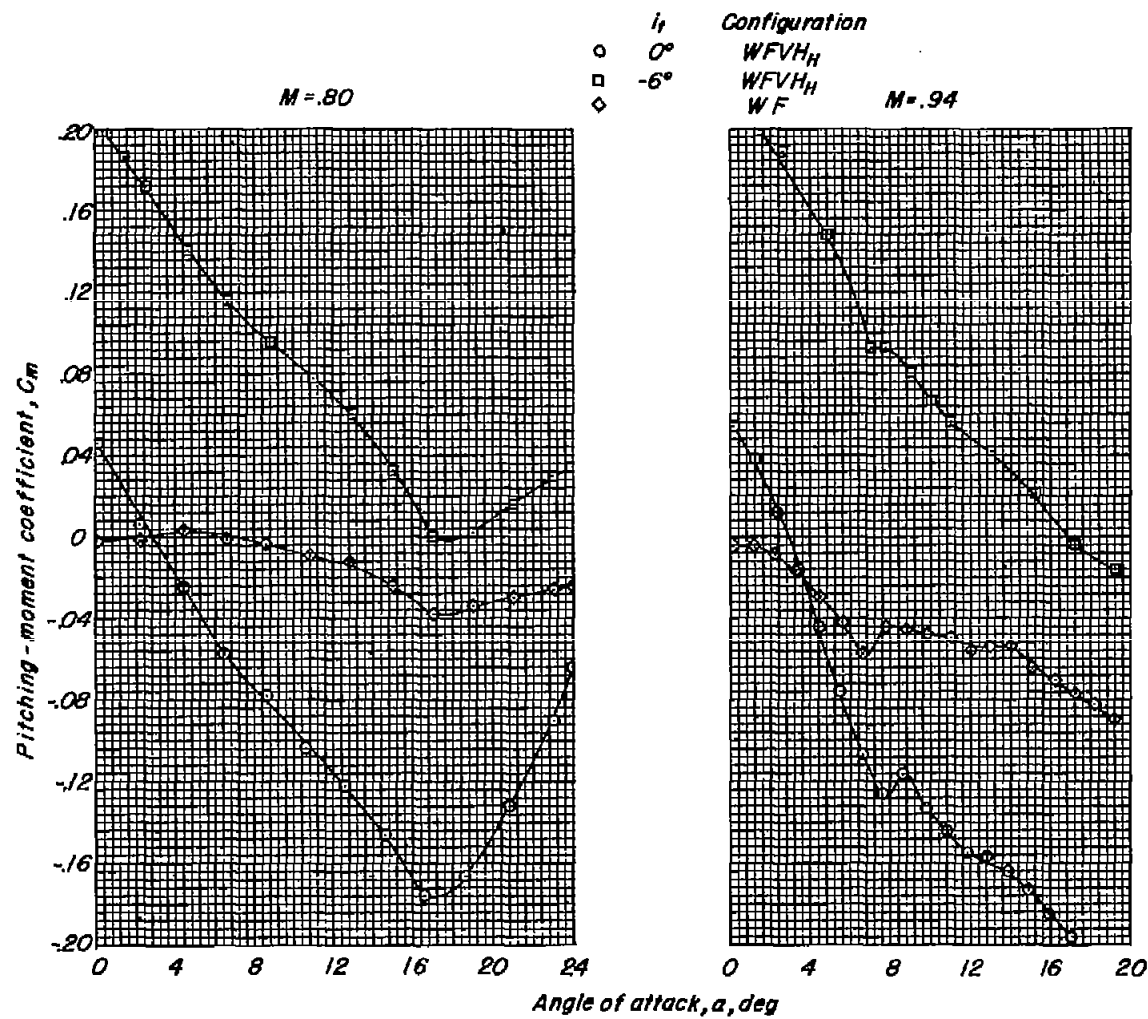
(c) Variation of  $C_m$  with  $\alpha$ ;  $i_t = 0^\circ$ .

Figure 13.- Continued.



(d) Effect of horizontal-tail incidence.

Figure 13.- Concluded.

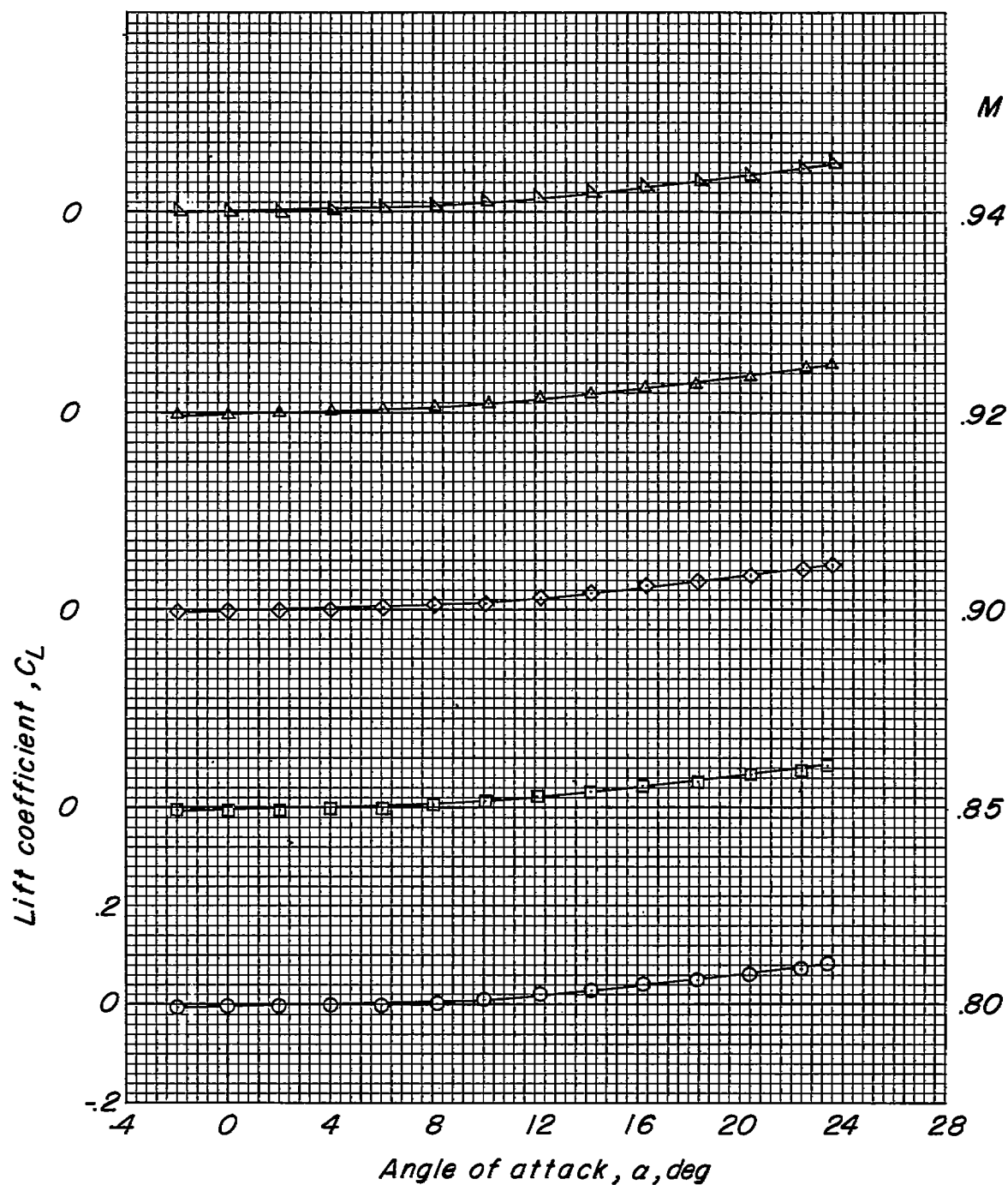
(a) Variation of  $C_L$  with  $\alpha$ .

Figure 14.- Aerodynamic characteristics of fuselage alone of fineness ratio 10.94.

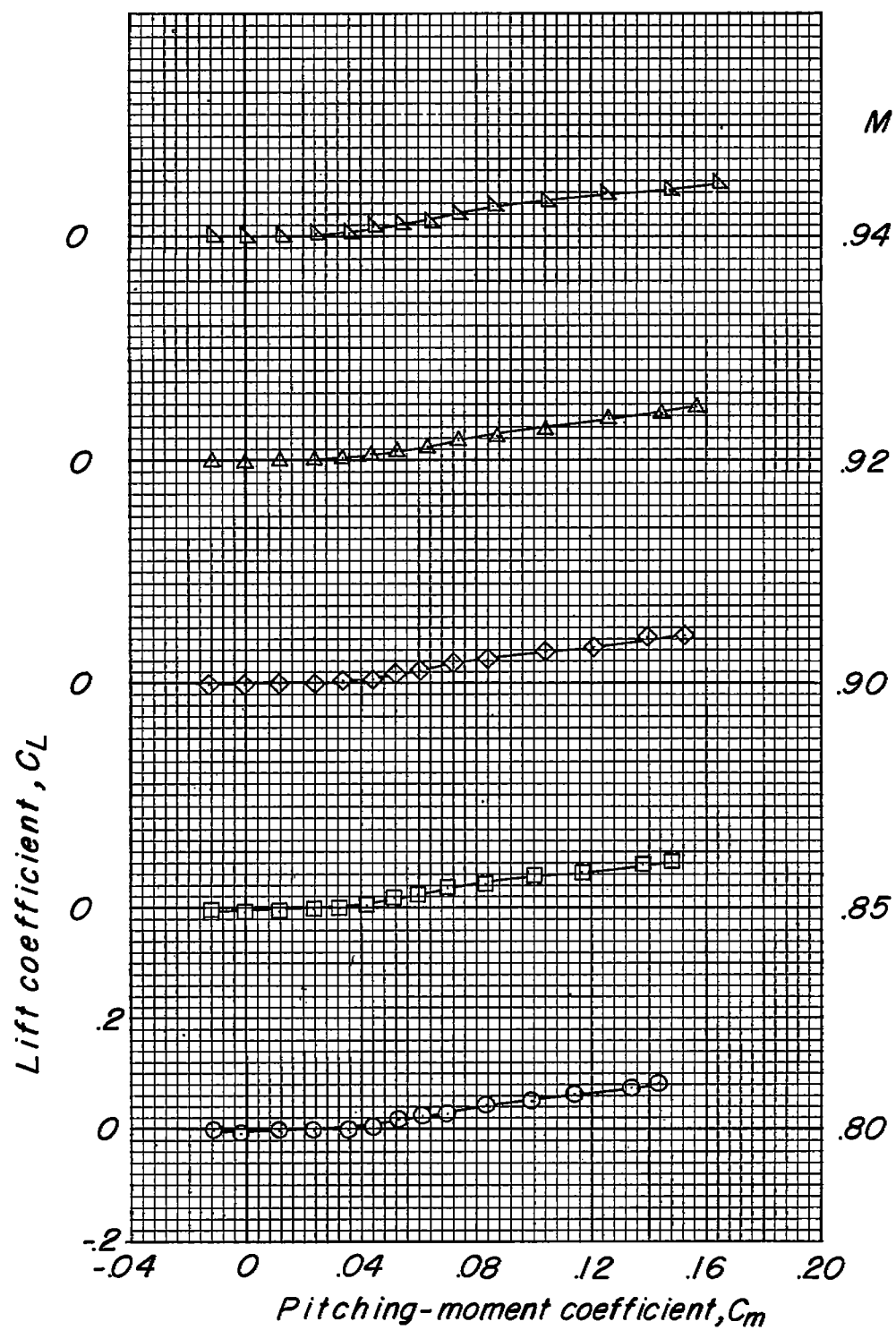
(b) Variation of  $C_L$  with  $C_m$ .

Figure 14.- Continued.

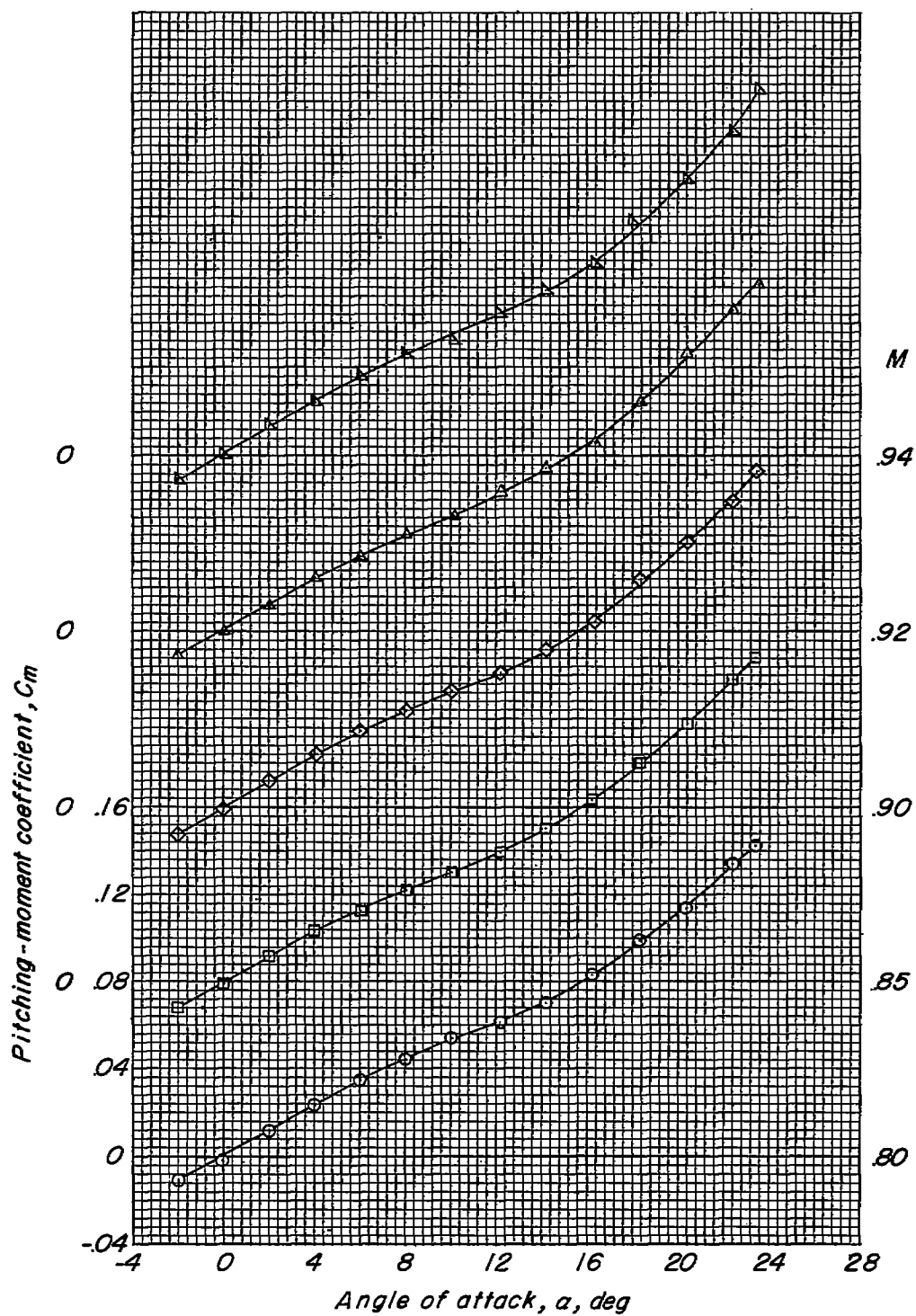
(c) Variation of  $C_m$  with  $\alpha$ .

Figure 14.- Concluded.

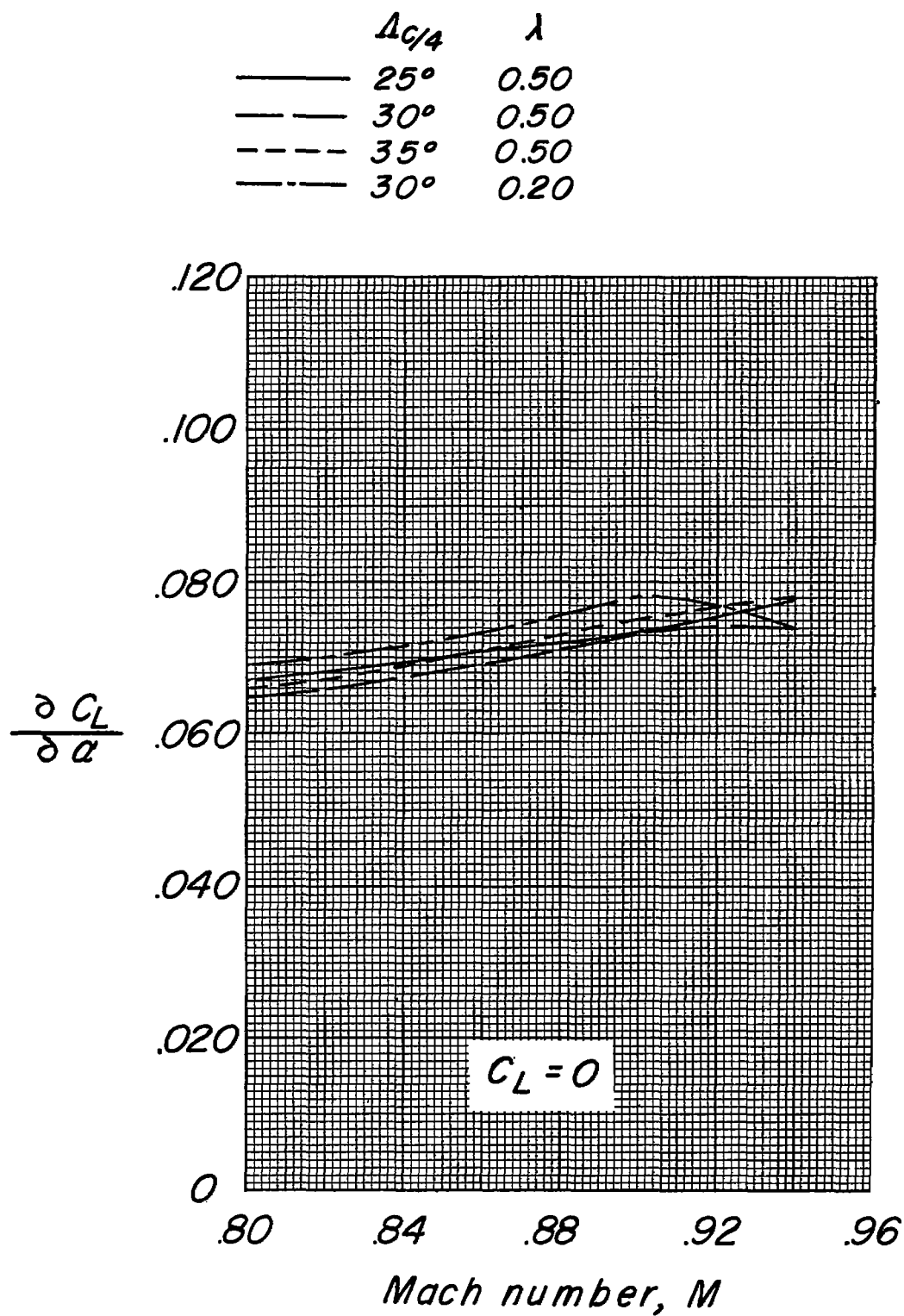


Figure 15.- Effect of wing plan form on the lift-curve slope of various wing-fuselage configurations.

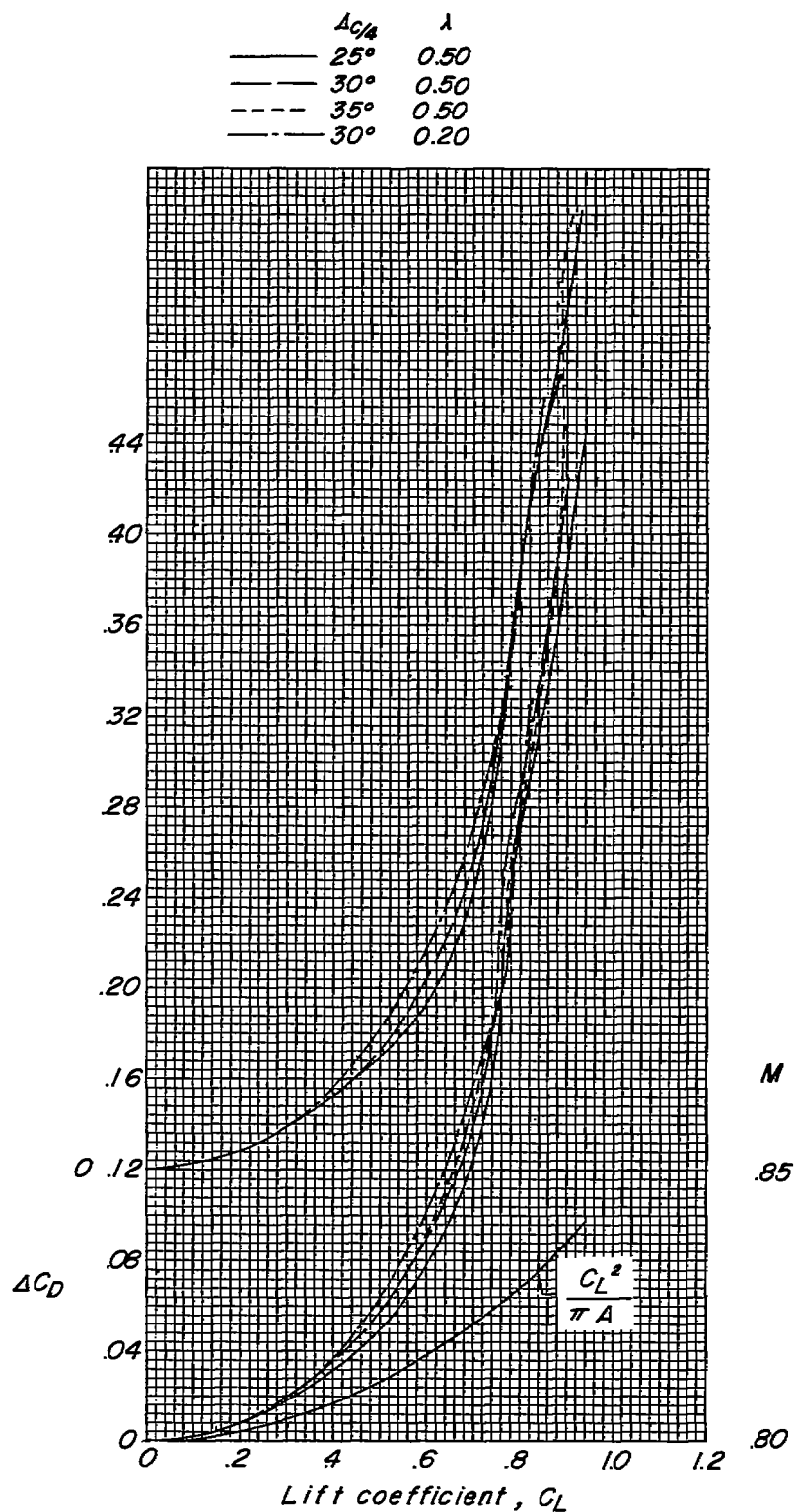


Figure 16.- Effect of wing plan form on the drag due to lift for various wing-fuselage configurations.

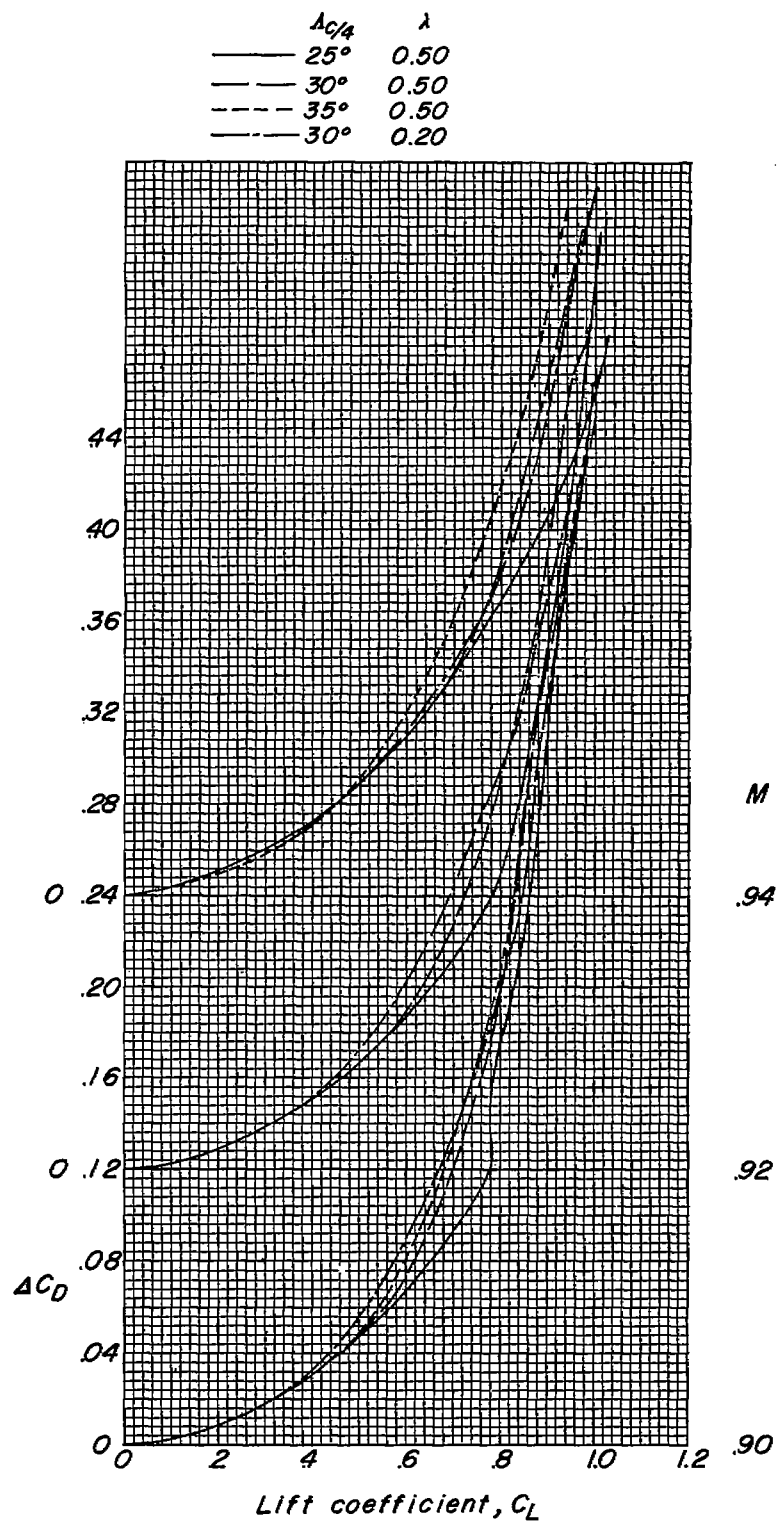
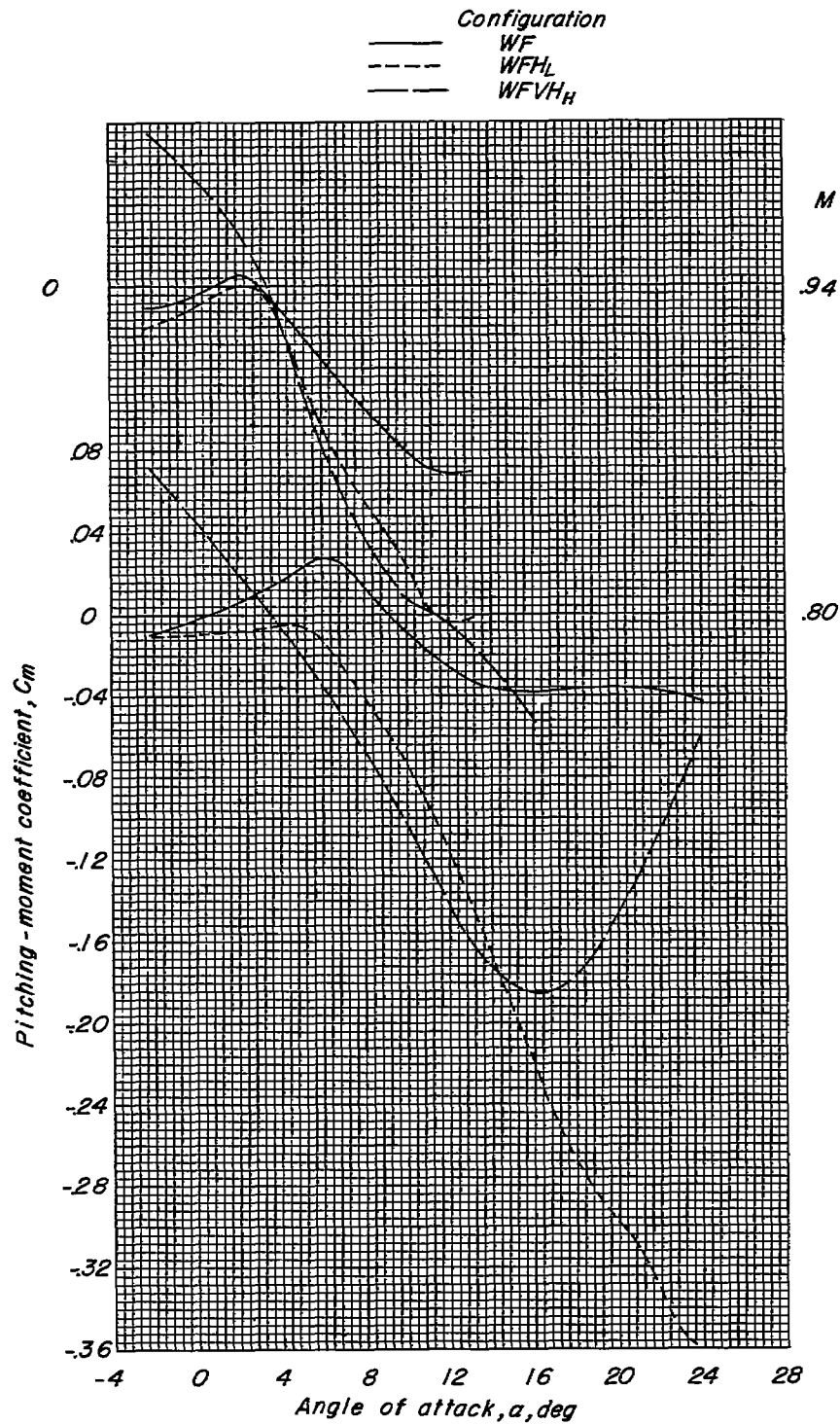
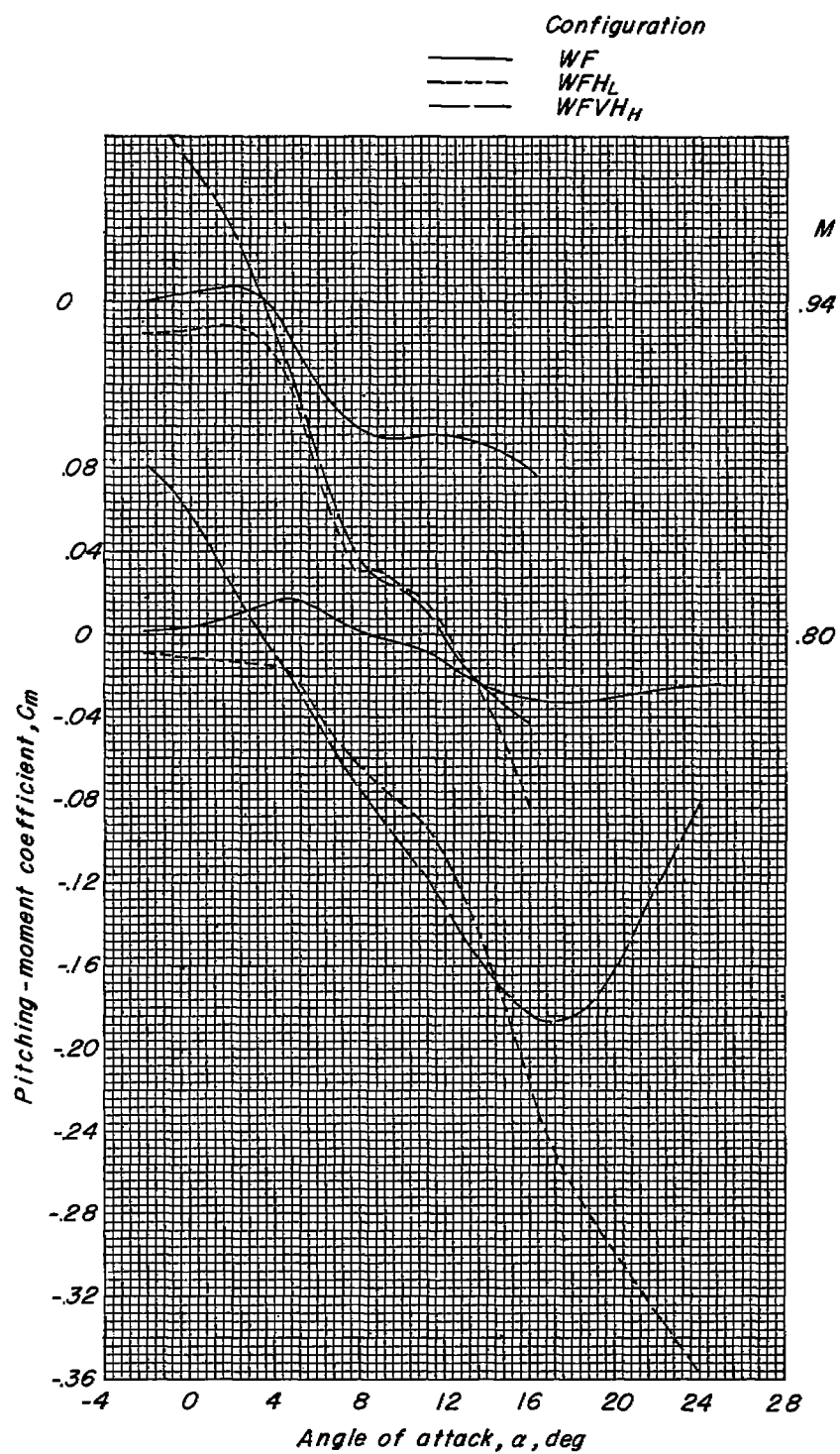


Figure 16.- Concluded.



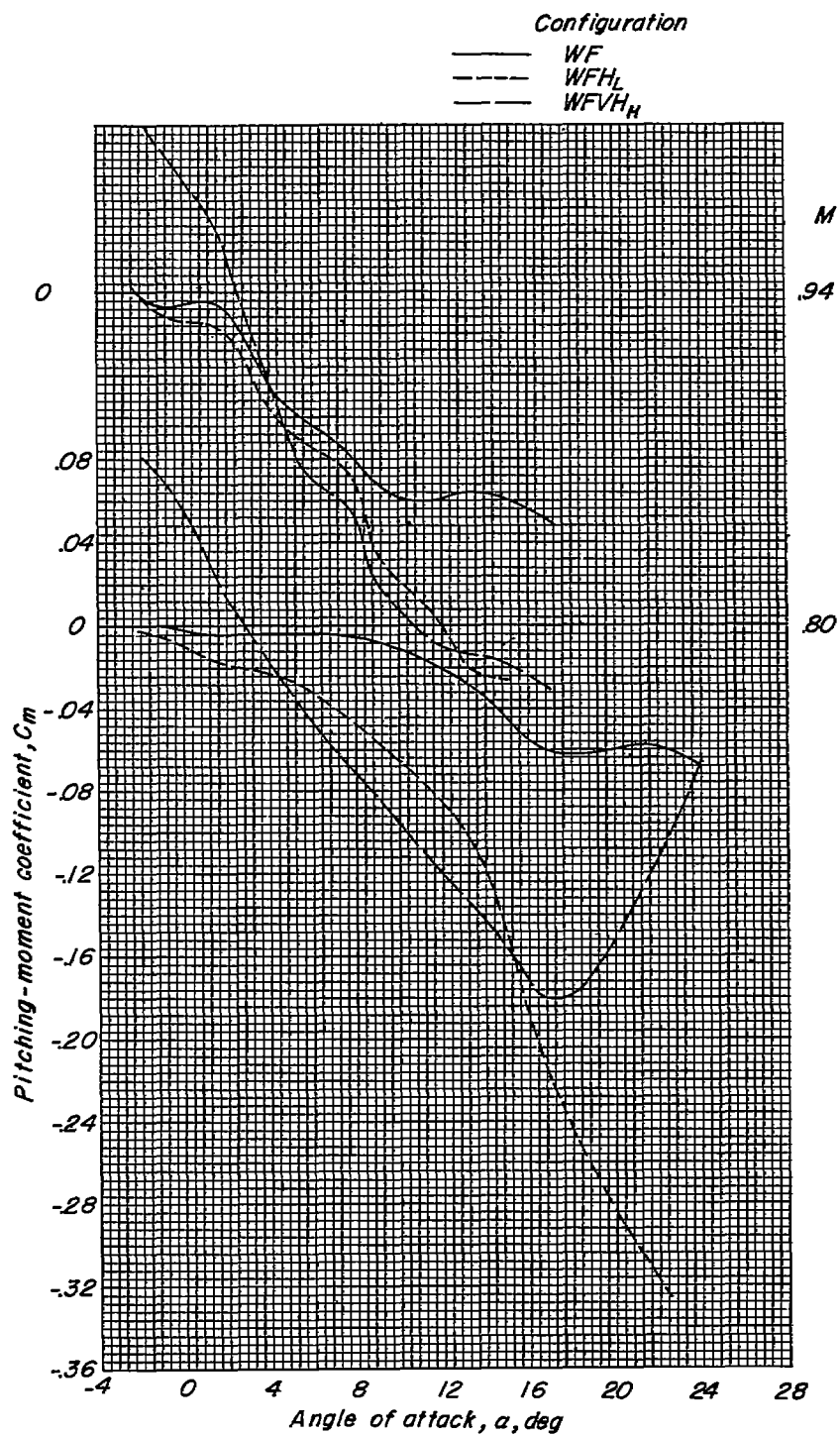
(a)  $\Lambda_c/4 = 25^\circ$ ;  $\lambda = 0.50$ .

Figure 17.- Effect of tail height on pitching moment.  $i_t = 0^\circ$ .



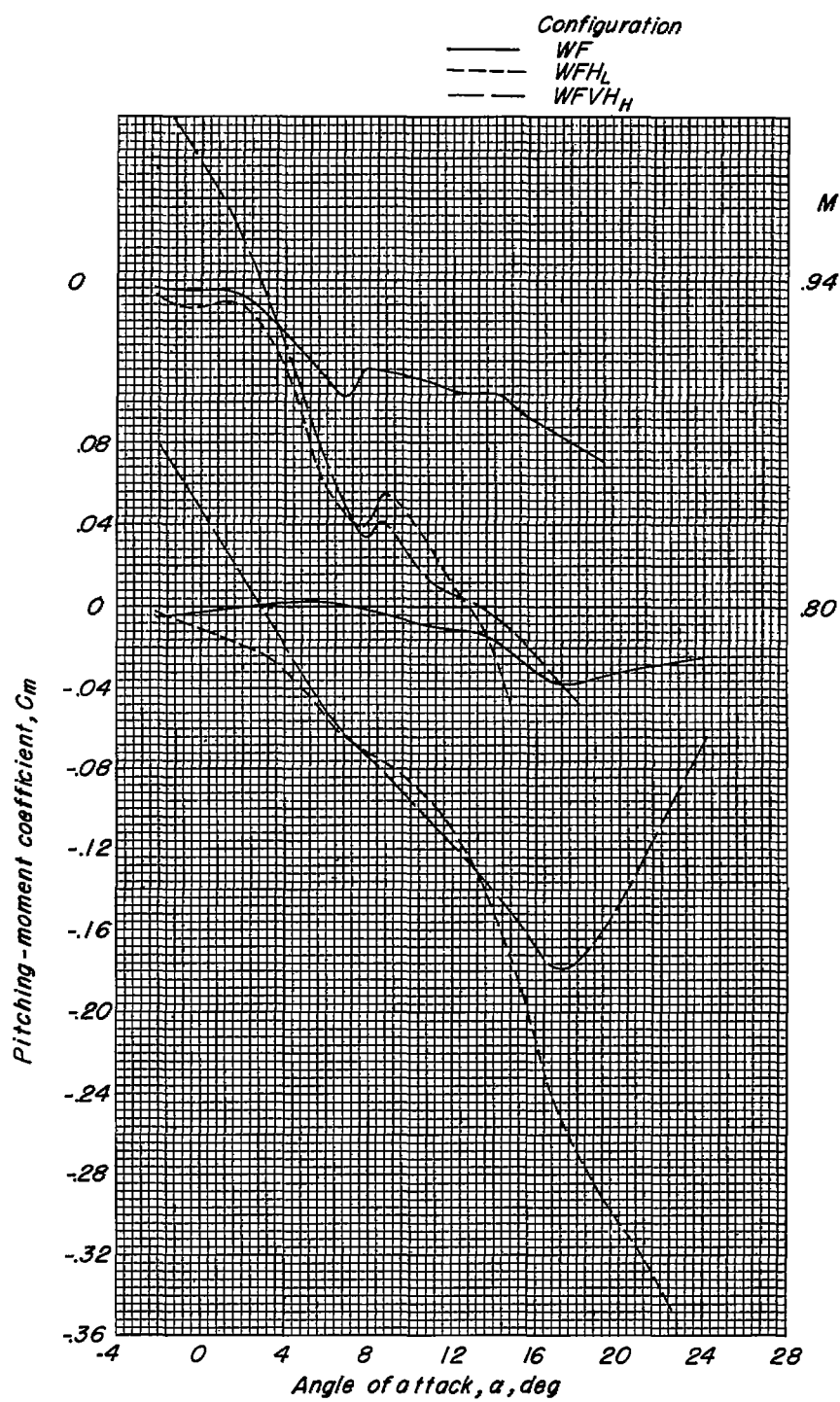
(b)  $\Lambda_c/4 = 30^\circ$ ;  $\lambda = 0.50$ .

Figure 17.- Continued.



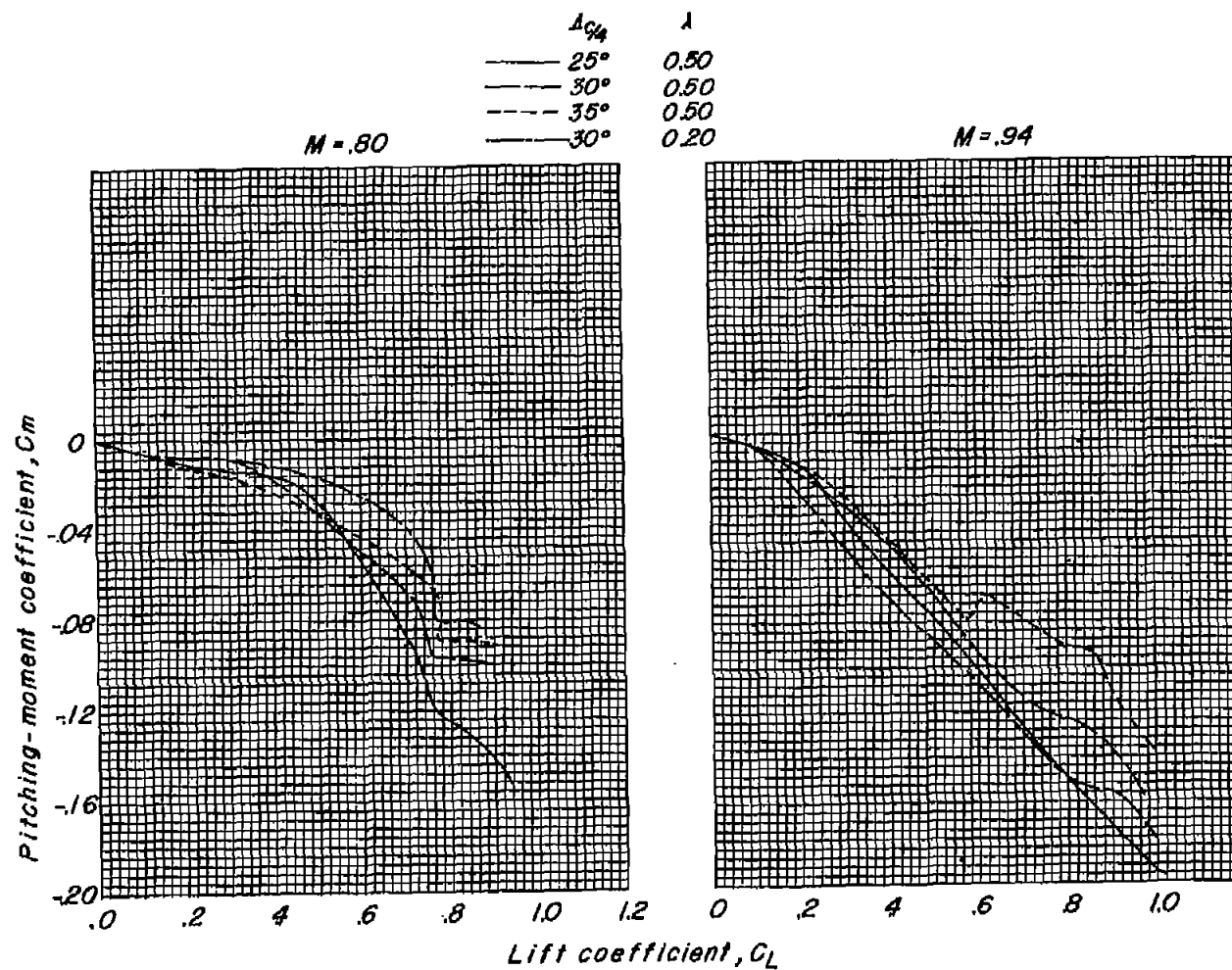
(c)  $\Lambda_c/4 = 30^\circ$ ;  $\lambda = 0.20$ .

Figure 17.- Continued.



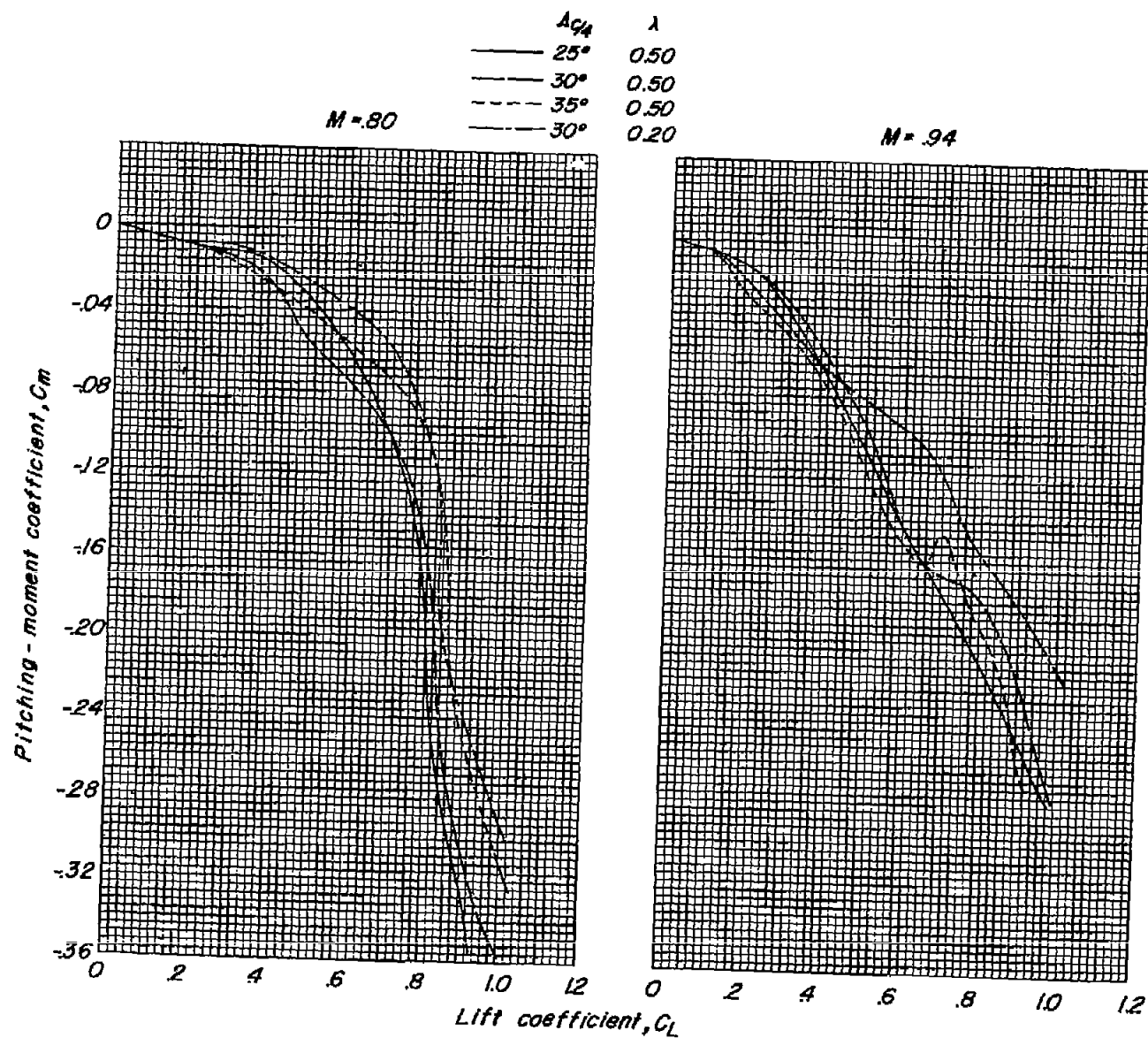
(d)  $\Lambda_c/4 = 35^\circ$ ;  $\lambda = 0.50$ .

Figure 17.- Concluded.



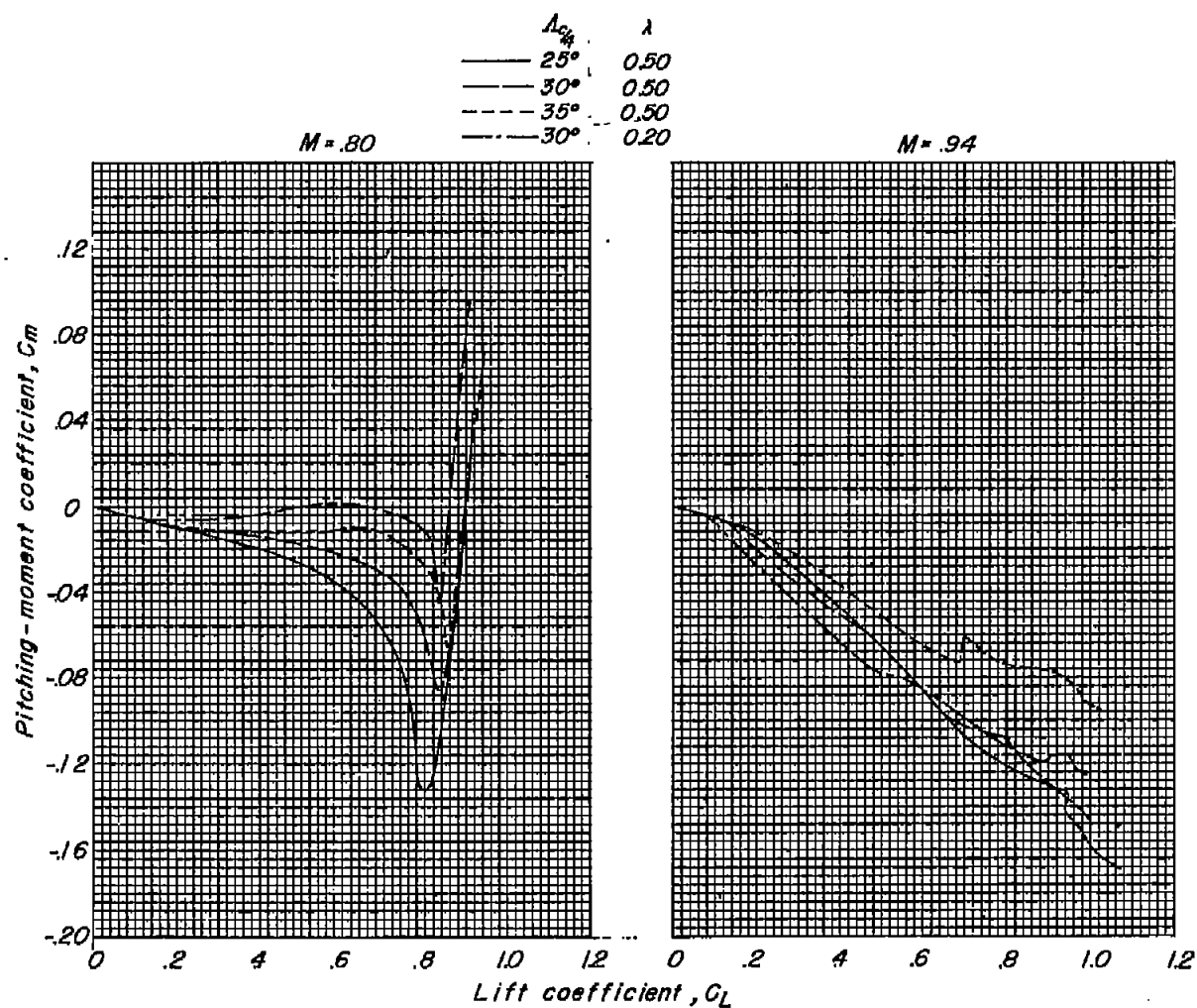
(a) Wing-fuselage configuration.

Figure 18.- Effect of tail height and wing plan form on the shape of the pitching-moment curves.  $i_t = 0^\circ$ .



(b) Wing-fuselage-low-tail configuration.

Figure 18.- Continued.



(c) Wing-fuselage-high-tail configuration.

Figure 18.- Concluded.

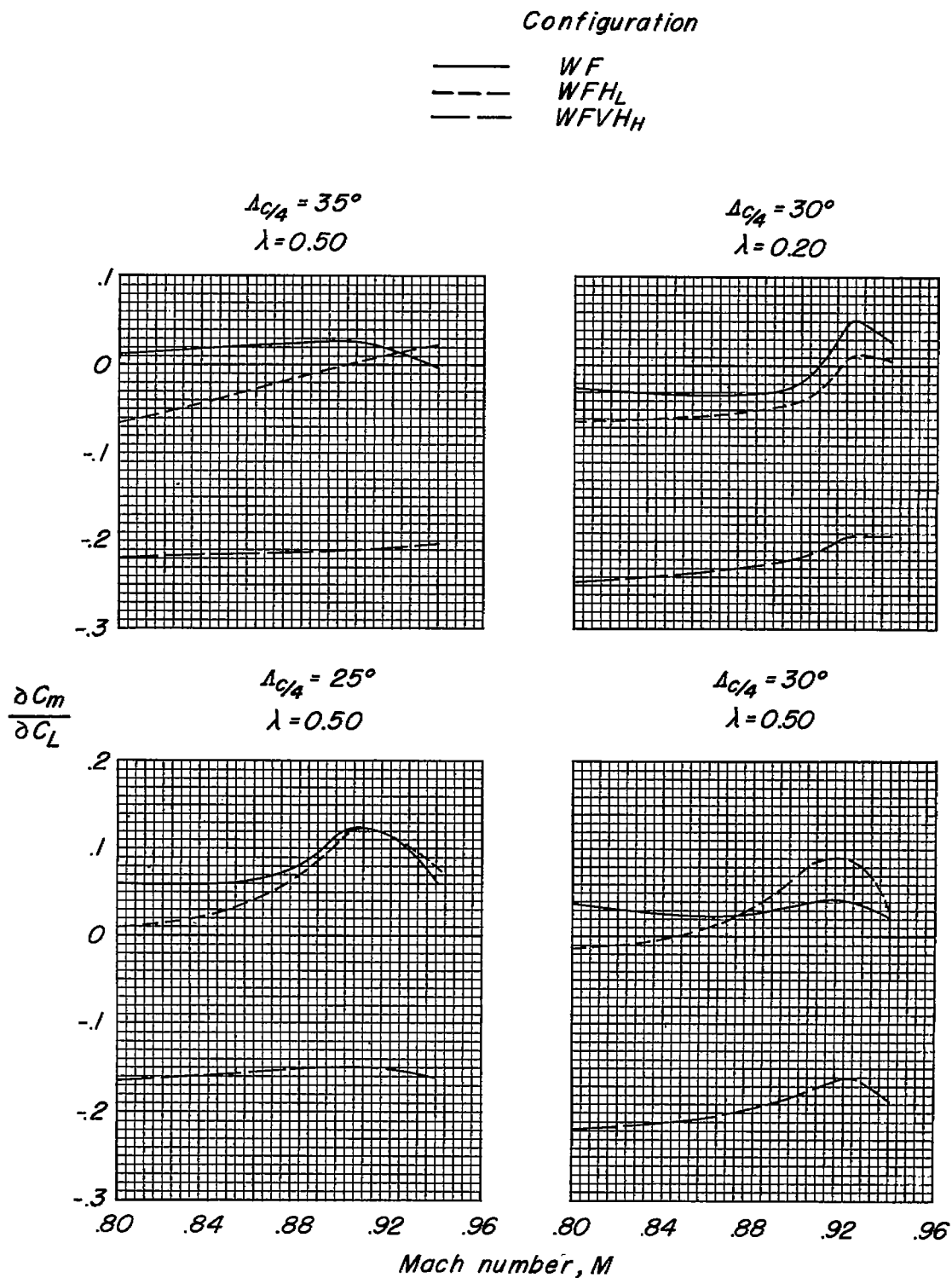


Figure 19.- Effect of tail height on the aerodynamic center ( $C_L = 0$ ) for various wing plan forms.  $i_t = 0^\circ$ .